HHS Public Access

Author manuscript

Nat Cell Biol. Author manuscript; available in PMC 2023 April 06.

Published in final edited form as:

Nat Cell Biol. 2022 October ; 24(10): 1475–1486. doi:10.1038/s41556-022-00999-5.

Murine foetal liver supports limited detectable expansion of life-long haematopoietic progenitors

Miguel Ganuza[1,5,6], **Trent Hall**[1], **Jacquelyn Myers**[4], **Chris Nevitt**[1], **Raúl Sánchez-Lanzas**[5], **Ashley Chabot**[1], **Juan Ding**[2], **Emilia Kooienga**[1], **Claire Caprio**[1], **David Finkelstein**[3], **Guolian Kang**[2], **Esther Obeng**[4], **Shannon McKinney-Freeman**[1,6]

[1]Department of Hematology, St. Jude Children's Research Hospital, Memphis, TN, 38105, USA

[2]Department of Biostatistics, St. Jude Children's Research Hospital, Memphis, TN, 38105, USA

[3]Department of Computational Biology, St. Jude Children's Research Hospital, Memphis, TN, 38105, USA

[4]Department of Oncology, St. Jude Children's Research Hospital, Memphis, TN, 38105, USA

[5]Centre for Haemato-Oncology, Barts Cancer Institute, Queen Mary University of London, London, EC1M 6BQ, United Kingdom

Abstract

Current dogma asserts that the fetal liver (FL) is an expansion niche for recently specified hematopoietic stem cells (HSCs) during ontogeny. Indeed, between embryonic day of development (E)12.5 and E14.5, the number of transplantable HSCs in the murine FL expands from 50 to about 1000. Here, we used a non-invasive, multi-color lineage tracing strategy to interrogate the embryonic expansion of murine hematopoietic progenitors destined to contribute to the adult HSC pool. Our data show that this pool of fated progenitors expands only two-fold during FL ontogeny. Although Histone2B-GFP retention in vivo experiments confirmed significant proliferation of phenotypic FL-HSC between E12.5 and E14.5, paired daughter-cell assays revealed that many mid-gestation phenotypic FL-HSCs are biased to differentiate, rather than self-renew, relative to phenotypic neonatal and adult bone marrow HSCs. In total, these data support a model in which the FL-HSC pool fated to contribute to adult blood expands only modestly during ontogeny.

Editor summary:

[6]Corresponding authors: M.G.: m.ganuza@qmul.ac.uk. S.M.-F.: shannon.mckinney-freeman@stjude.org.

Author Contributions

M.G. designed the study, treated mice, performed single cell assays, cell division history experiments, bone marrow and fetal liver transplants, collected and analysed data, and wrote the paper. T.H. contributed to experimental design, performed bone marrow and fetal liver transplants, collected and analysed data. A.C. contributed to experimental design, collected and analysed *Confetti* mice. E.K. processed and stained hematopoietic colonies. C.C. contributed mouse colony management. R.S-L performed and analysed single cell assays. C.N. carried out and analysed PVA cultures. J.M. and E.O. performed transcriptional analyses of FL-HSC and Adult HSCs. J.D., D.F. and G.K. performed statistical analyses. S.M.-F. designed the study, analysed data, and wrote the paper. All authors discussed the results and commented on the manuscript.

Declaration of Interests

The authors declare no competing interests.

Ganuza et al. report that fetal liver hematopoietic stem cells (HSCs) are largely biased to differentiation rather than self-renewal, resulting in a modest expansion of the HSC pool with contribution to adult hematopoiesis.

Keywords

Hematopoietic ontogeny; fetal liver; hematopoietic stem cells; differentiation; self-renewal; expansion niche

Introduction

HSCs produce most blood throughout life. In mice, between E8.5 and E10.25, a subset of endothelial cells (*i.e.* hemogenic endothelium) undergo an endothelial to hematopoietic transition (EHT) to generate the first HSCs capable of reconstituting blood when transplanted into adults[1–7]. Between E10.5 and E11.5, only 1-2 transplantable HSCs per embryo are detected[1–3]. These newly emerged HSCs migrate to fetal liver (FL), where they presumably proliferate and establish the HSC pool that supports life-long hematopoiesis[1–3, 8–13]. It is estimated that between E11.5-E15.5, HSCs expand about 1000-fold, presumably via self-renewal in the FL, as the FL-HSC pool is cycling[1–3, 8–13]. HSCs complete their migration to the bone marrow (BM) by post-natal day 8 (P8) and enter quiescence by P27[14–19]. Because FL harbors cycling HSCs, many studies have focused on the FL searching for exogenous factors that support HSC expansion [9, 20–29]. Indeed, ANGIOPOIETIN-3, WNTs, EPHRIN2A, OSM, CSF1, THPO, EPO, IGF1, SCF/KITL, CXCL12, ANGPTL2 and ANGPTL3 are present in the FL niche and implicated in HSC maintenance and function[22, 27, 30–35]. However, to our knowledge, despite expression at the supposed time and place of HSC expansion, none of these proteins are used clinically to expand HSCs before transplantation. Efficient HSC *ex vivo* expansion still constitutes an unmet clinical need [36–38].

Recent assessments of the temporal dynamics and clonal complexity of the hematopoietic system call the model of FL HSC expansion into question. Whole-genome sequencing, telomere length, and replication rates suggest that human HSC numbers mainly increase between birth and adolescence, which is inconsistent with a FL expansion model [39–41]. We recently demonstrated that lifelong murine hematopoiesis is founded by hundreds of blood progenitors throughout mammalian ontogeny [7, 28]. By E8.5, >500 progenitors fated to contribute to life-long hematopoiesis are present in the embryo, which represents about half of the 1,000 transplantable FL-HSCs seen at E14.5 [1–3, 8–10]. These data provocatively suggest that embryonic HSCs with life-long blood potential may not massively expand in the FL.

To tackle this conundrum, we interrogated the magnitude and developmental timing of HSC and HSC progenitor expansion in the FL and neonates. Towards this, we employed multi-color *ROSA26-Confetti* reporter (*i.e. Confetti* allele) based lineage-tracing combined with a tamoxifen (TAM) regulated *Ubiquitin-ERT2-Cre* allele[7, 42–44], a doxycycline (DOX)-inducible *H2B-GFP* allele[45, 46] and functional paired-daughter cell assays to assess the scale of expansion, the absolute number of cell divisions and the balance of symmetric

versus asymmetric cell divisions amongst hematopoietic progenitors during ontogeny. Cumulatively, our results support a model in which many cell divisions undertaken by FL-HSCs fail to expand the cells fated to contribute to the adult HSC pool. Instead, many FL-HSCs display a strong bias for differentiation, rather than symmetric self-renewal. These findings fundamentally alter our understanding of FL's role during embryonic haematopoiesis.

Results

Fetal HSCs fated to adult haematopoiesis modestly expand

We showed previously that only about 550 nascent blood stem and progenitor cells genetically labelled by *Vav1*-Cre contribute to adult blood[7]. *Vav-1* becomes expressed in hematopoietic stem and progenitor cells (HSPCs) shortly after HSC emergence. Between E11.5-E14.5, *Vav1-Cre* labels ~30% of FL-HSPCs but ultimately labels 80% of adult blood, indicating that *Vav1-Cre*-labeling is either not saturating by E14.5 or that *Vav1-Cre* expression selectively marks those HSPC fated to contribute to adult blood [7], making it difficult to draw definitive conclusions regarding the magnitude of FL-HSPC expansion in these prior studies.

Thus, to better understand the timing and magnitude of HSC expansion during ontogeny, we utilized *ROSA26*$^{+/Confetti}$*; Ubiquitin*$^{+/ERT2\text{-}Cre}$ (*Conf-Ubiq*$^{ERT2\text{-}Cre}$) mice to estimate numbers of cells contributing to adult blood during mouse ontogeny [7, 42]. We initially focused on the FL stage of HSC development, as this is when recently specified HSCs are presumed to expand dramatically, which our previous analyses failed to detect [1–3, 7–10]. Our previously reported non-invasive approach to study clonal dynamics of the blood during mouse ontogeny is based on the random labelling of blood precursors with the Cre-recombinase (CRE) inducible *Confetti* allele[7, 42]. This allele consists of three cassettes flanked by *loxP* sites that encode four distinct fluorescent proteins (*i.e.* GFP, YFP, RFP and CFP, Extended Data Figure 1Ai) [43]. CRE activity recombines the *Confetti* allele to randomly label cells, and their progeny, with a single fluorophore [43]. The mouse-to-mouse-variance (MtMV) in the distribution of *Confetti* colors inversely correlates with the number of initially labelled cells and thus can be used to estimate their numbers (Extended Data Figure 1Aii)[7, 42]. As cells are labelled via genetic rearrangement, the MtMV in *Confetti* labelling is preserved in the progeny. Thus, the MtMV of *Confetti* labelling in the blood of a cohort of mice can be used to estimate the number of initially labelled blood precursors during development[7, 42].

To interrogate the expansion of HSCs and HSC progenitors that contribute to life-long haematopoiesis during FL ontogeny, *Conf-Ubiq*$^{ERT2\text{-}Cre}$ embryos or neonates were exposed to tamoxifen (TAM) at E12-E14 or postnatal day 1 (P1) (Figure 1A–B). We previously showed that CRE is active for less than 24 hours post-TAM treatment [7]. A cohort of *ROSA26*$^{+/Confetti}$*; VE-Cadherin*$^{+/Cre}$ (*Conf-VE*^{Cre}) mice was used to verify initial numbers of hemogenic endothelial progenitors at E8-E10 (Figure 1A) [7]. Progenitor numbers contributing to adult haematopoiesis during each developmental window was estimated by calculating the MtMV of P60 and P180 peripheral blood (PB) for each mouse cohort in the myeloid and lymphoid lineages (B and T), as well as in BM HSPCs

(*i.e.* HSCs, Lineage^{-}Sca-1^{+}c-Kit^{+} [LSK] CD150^{+}CD48^{-}; multipotent progenitors [MPPs], LSK CD135^{+}; common myeloid progenitors [CMP], LSK CD32/16^{Low}CD34^{+}; common lymphoid progenitors [CLP], Lineage^{-}c-Kit^{Low}Sca-1^{Low}CD127^{+}; megakaryocyte-erythroid progenitors [MEP], LSK CD32/16^{-}CD34^{-}; granulocyte-myeloid progenitors [GMP], LSK CD32/16^{-}CD34^{-}) (Figure 1C–D, Supplementary Table 1, Extended Data Figures 1B–C, 2–3).

MtMV analysis in *Conf-VE^{Cre}* mice revealed 908 (95% confidence interval (CI) [887, 929]) and 1,032 endothelial progenitors (95% CI [993, 1,074]) contributing to PB at P60 and P180, respectively (Figure 1Ci–ii, Extended Data Figure 3, Supplementary Table 1). Analysis of *Conf-Ubiq$^{ERT2-Cre}$* cohorts exposed to TAM between E12 and E14 indicated 2,551 (95% CI [2,312, 2,815]) life-long blood progenitors at P60 and 2,744 (95% CI [2,734, 2,754]) at P180 (Figure 1Ci–ii, Extended Data Figure 3, Supplementary Table 1). Thus, life-long blood progenitors expand about 2.7-fold between E10-E15, suggesting 1-2 symmetric divisions of this cell pool. Contributing progenitor numbers to P60 PB further increased to 4,505 (95% CI [3,086, 6,578]) by P1. This increase was not apparent at P180 (1,825, 95% CI [1,617, 2,060]), suggesting transient contributors in early adult life (Figure 1Ci–ii, Extended Data Figure 3, Supplementary Table 1) [47]. In sum, between E10 and P1 there is a modest increase (*i.e.* 1.8-fold) in the number of progenitors contributing to P180 PB.

As we did not observe a large expansion in FL HSPCs contributing to adult blood, we next examined expansion during post-natal life. Here, *Conf-Ubiq$^{ERT2-Cre}$* cohorts of mice were TAM-treated at P8-P9, P14-P15 and P21-P22 and then analysed at P60 and P180 for *Confetti* labelling (Figure 1A, Ci–ii, Extended Data Figure 3, Supplementary Table 1). P60 PB contributors continued their modest expansion during the post-natal period: from 4,505 (95% CI [3,086, 6,578]) at P1 to 8,021 (95% CI [4,287, 15,006]) at P9, 5,437 (95% CI [4,116, 7,181]) at P15 and 13,846 (95% CI [8,630, 22,217]) at P22 (Figure 1Ci, Extended Data Figure 3A, Supplementary Table 1). Although these estimates fall outside the optimal quantitative range of MtMV (*i.e.* 50-2,500) [7], they none-the-less indicate a qualitative gradual expansion of progenitors that persists into early adulthood during this period (Supplementary Table 1) [7]. When P180 PB was examined, the numbers of life-long progenitors shifted from 1,825 (95% CI [1,617, 2,060]) at P1 to 4,023 (95% CI [2,748, 5,888]) at P9, 13,643 (95% CI [8,371, 22,233]) at P15 and 23,016 (95% CI [13,536, 39,136]) at P22 (Figure 1Cii, Extended Data Figure 3B, Supplementary Table 1). Again, the decline in P1 and P9 contributors to P180 PB (versus P60 PB) likely reflects the dynamics of progenitor recruitment and loss during young adulthood and transient progenitors capable of PB contribution for many months before exhaustion [48–50].

To directly assess numbers of hematopoietic progenitors across mouse ontogeny contributing to the adult HSC pool, we analysed the BM of 6-month-old TAM-treated *Conf-Ubiq$^{ERT2-Cre}$* mice (Figure 1Di, Supplementary Table 1). Here, about 848 endothelial progenitors (95% CI [766, 938]) and 1,761 E12-E14 progenitors (95% CI [1,285, 2,414]) actively contribute to P180 phenotypic HSCs. As in PB, the number of contributors to the adult HSC pool increased only 2.1-fold between E10.5 to E15.5. This stands in stark contrast to the 20-fold increase in repopulating units (RUs) seen in classic transplantation

studies during the same period [1–3, 8–10]. One possibility is that 'immature' HSCs (pre-HSCs) that lack adult repopulating potential acquire this potential overtime in the FL. Surprisingly, only 1,886 P1 HSC-progenitors (95% CI [1,848, 1,925]), 2,125 (95% CI [2,000, 2,258]) P8-P9 HSC-progenitors, 2,983 (95% CI [2,738, 3,250]) P14-P15 HSC-progenitors and 5,753 (95% CI [5,521, 5,995]) P21-22 HSC-progenitors contributed to the HSC pool at P180 (Figure 1Di, Supplementary Table 1). Thus, progenitors fated to contribute to the adult HSC pool barely expanded between E15-P9 (p-value=0.6), while expanding 1.4-fold between P9-P15 and 1.7-fold between P15-P21 (as suggested by non-overlapping 95% CI). These data reveal a steady increase in HSC clonal complexity between P1-P21. Importantly, the number of detected HSC contributors fell in the optimal MtMV range (*i.e.* 50-2,500) until P9, allowing us to quantitatively assess the dynamics of HSC contributors until P9 and qualitatively visualize steady expansion thereafter (Supplementary Table 1) [7].

Phenotypic FL-HSC undergo many cell divisions during ontogeny

RUs expand from 50-60 at E12.5 to >1,000 at E14.5, a 20-fold increase that should require about five symmetric divisions as a population [1–3, 8–10, 12]. The cellular mechanism behind this increase in RUs is assumed to be symmetric division of transplantable HSCs [1, 2, 8–10, 13, 15, 51, 52]. However, to our knowledge, the number and nature of cell divisions in the FL-HSC pool has not been investigated. To address this, we employed *ROSA26$^{rtTA/rtTA}$;pTRE-H2BGFP$^{+/GFP}$ (TRE-H2B-GFP)* mice (Figures 2–3), which allow for DOX-inducible H2B-GFP (Figure 2A) [45, 46]. Following a DOX pulse, DNA-integrated H2B-GFP is distributed between daughters as labelled cells divide, halving the median fluorescent intensity (MFI) of GFP (*i.e.* $y_N/y_o=2^{-N}$, where y_N=MFI after N divisions; y_o=MFI before cell division; N= number of cell divisions) [45, 53]. Hence, $N= \log_2(y_o/y_N)$, suggesting that the number of divisions between two timepoints can be calculated by measuring the shift in GFP MFI.

To confirm a correlation between GFP MFI loss after DOX removal and the number of cell divisions, mouse embryonic fibroblasts (MEFs) were immortalized from four independent E13.5 *TRE-H2B-GFP* embryos. Most *TRE-H2B-GFP* MEFs were GFP$^+$ after DOX exposure (Figure 2B–C). However, we observed large variability in the median GFP MFI and the breadth of GFP expression between individual cell lines, even after 15 days of DOX (Figure 2C). As discrete GFP$^+$ peaks could not be correlated with a specific number of cell divisions after DOX removal, we employed $N= \log_2(y_o/y_N)$ to estimate numbers of cell divisions. MEFs were treated with DOX for three days to saturate H2B-GFP expression and then plated without DOX and counted every three days while monitoring GFP MFI (Figure 2D). Division kinetics varied between *TRE-H2B-GFP* cell lines: some divided rapidly while others more slowly (Figure 2D). To estimate numbers of cell divisions (N), the loss of GFP MFI (y_0/y_N) upon DOX removal was calculated each day by measuring the GFP MFI in pulsed immortalized cells (y_N) and their internal +DOX controls (y_o) (Figure 2D). Untreated controls remained GFP$^-$ (Figure 2C). A comparison of the number of divisions calculated by cell counting (actual number of divisions: N_a) and the estimated values based on H2B-GFP MFI loss revealed that $N_a= e^{(-0.757+0.541*N)}$ accurately calculates up to 6.5 cumulative cell divisions (Figure 2E). Further dilution of GFP MFI due to cell division is undetectable in this system, which plateaus around eight 'estimated' cell divisions regardless of the 'actual'

number of divisions (*e.g.* ~5,000 cell cumulative divisions recorded for clone #C 14 days post-DOX removal, Figure 2E).

To estimate the number of divisions undergone by phenotypic HSCs between E12.5-E14.5, *ROSA26*$^{rtTa/rtT}$*; pTRE-H2BGFP*$^{+/GFP}$ mice were treated with DOX *in utero* from E0.5-E11.5 (Figure 3B). We estimated that active H2B-GFP-labeling continues for about 24 hours after DOX removal (Extended Data Figure 4). Thus, under this treatment regimen H2B-GFP labelling continues until E12.5.

First, to verify H2B-GFP labelling of recently specified E12.5 HSC and HSC progenitors, the aorta-gonad-mesonephros region (AGM) and FL were examined from individual DOX-treated *TRE-H2B-GFP* mice at E12.5 (Figure 3A–B, Extended Data Figure 5A). Similar to DOX-treated *TRE-H2B-GFP* MEFs, the GFP MFI of E12.5 CD45$^+$c-Kit$^+$Lin$^-$ cells varied widely embryo-to-embryo and a broad range of GFP expression was observed within each embryo (Figure 3B). On average, the efficiency of H2B-GFP labelling of E12.5 AGM/FL CD45$^+$c-Kit$^+$Lin$^-$ cells was 39% (Figure 3Bii). Similarly, E14.5 phenotypic FL-HSCs (CD150$^+$CD48$^-$Lin$^-$Sca-1$^+$c-Kit$^+$) isolated from DOX-treated embryos (between E0.5-E14.5) displayed variable GFP MFI embryo-to-embryo, a broad range of GFP expression, and some unlabelled cells (Figure 3C). GFP MFI was similar in E12.5 CD45$^+$c-Kit$^+$Lin$^-$ cells exposed to DOX between E0.5-E11.5 and E14.5 HSCs exposed to DOX from E0.5-E14.5 (GFP MFI = 6,223±3,023 and 6,886±3,286, respectively), suggesting that H2B-GFP labelling saturates by E12.5 (Figures 3B–C).

To estimate the number of cell divisions undergone by newly specified HSCs and immature HSC (*i.e.* E12.5 FL/AGM CD45$^+$c-Kit$^+$ Lin$^-$ cells) between E12.5-E14.5, the GFP MFI (y_N) of GFP$^+$ phenotypic FL-HSCs was examined in E14.5 *TRE-H2B-GFP* embryos exposed to DOX from E0.5-E11.5 (n=20) and compared to the GFP MFI (y_o) of GFP$^+$ E12.5 AGM/FL CD45$^+$c-Kit$^+$ Lin$^-$ cells in *TRE-H2B-GFP* embryos exposed to DOX from E0.5-E11.5 (n=7) (Figure 3A–C). Average y_o was calculated (Average y_o=6223). To control for LASER variation between experiments, four different untreated and DOX-treated *TRE-H2B-GFP* immortalized lines were included as fluorescence intensity controls (Figures 3B–C). The number of divisions (N) of E12.5 CD45$^+$c-Kit$^+$ Lin$^-$ HSC progenitors between E12.5 and E14.5 was calculated for each embryo as $N= \log_2(y_o/y_N)$ and the number of actual divisions via $N_a= e^{(-0.757+0.541*N)}$. This population was thereby estimated to divided 4.1 times to generate the E14.5 HSC pool, which roughly coincides with the expected number of divisions based on RU expansion (Figure 3D). As expected, non-HSC CD45$^+$c-Kit$^+$ Lin$^-$ cells, which represent a mixture of committed HSPCs [54], divided more frequently, as nearly all H2B-GFP signal was lost from this population by E14.5 (Figure 3C).

E14.5 FL HSC-progenitors are biased towards differentiation

FL-HSCs are clearly highly proliferative (*i.e.* four cell divisions between E12.5-E14.5, Figure 3D) [10, 11, 13, 55]. Yet, we detected only a modest expansion between E10-E15.5 of the number of clones contributing to adult HSCs (*i.e.* 848 at E10 and 1,761 at E15.5) (Figure 1Di, Supplementary Table 1). Thus, we examined the nature of the cell divisions of phenotypic FL-HSCs using paired-daughter-cell assays. To first visualize the erythro-myeloid potential of E14.5 FL-HSCs and adult HSCs (CD150$^+$CD48$^-$Lin$^-$Sca-1$^+$c-Kit$^+$) we

cultured them as single cells in differentiation media (Figure 4A–B) [42, 56]. Interestingly, only 16% of E14.5 FL-HSC generated four lineages in this assay (*i.e.* megakaryocytes, erythrocytes, monocytes and granulocytes) while adult HSCs displayed more homogeneous potential: 59% yielded four lineages (p-value=4.7×10^{-5}) (Figure 4B).

Next, single E14.5 FL, P4 BM, P11 BM and P60 BM HSCs were cultured in expansion media until their first cell division [42, 56]. Each daughter cell was then individually replated in differentiation media for 14 days and scored for erythro-myeloid potential (Figures 4A, 4C–E) [42, 56]. If both daughters yielded four lineages, the division was scored as symmetric. If only one daughter yielded four lineages, the division scored as asymmetric. If each daughter cell yielded fewer than four lineages, but identical lineage potential, it was scored as symmetric differentiation. If both daughters disparately displayed fewer than four lineages, the division was scored as asymmetric differentiation (Figures 4C–E). Only 6% of E14.5 FL-HSCs underwent symmetric division, while 21% of P4-HSCs, 30% of P11-HSCs and 26% of P60-HSCs symmetrically divided, demonstrating significant enrichment for symmetric divisions in postnatal HSCs (p = 0.1, 0.01 and 0.04, respectively) (Figure 4E). These data suggest a gradual shift from symmetric differentiation, asymmetric cell division and asymmetric differentiation towards symmetric division during development. Importantly, many of the cell divisions of E14.5 FL-HSCs resulted in differentiation.

We next examined the effect of ANGPTL-3, a FL niche factor that supports the expansion of adult BM-HSCs, on FL-HSC division[22]. Adult BM-HSCs and FL-HSCs were cultured in the presence or absence of ANGPTL-3 under conditions that promote adult BM-HSC expansion (*i.e.* Extended Data Figure 5B–E) [38]. ANGPTL-3 resulted in a moderate, albeit not statistically significant, increase in adult BM-HSC expansion. Surprisingly, FL-HSCs did not expand in PVA cultures, regardless of ANGPTL-3 treatment. These data underscore cell-intrinsic differences between FL and BM-HSCs. We also tested the effect of ANGPTL-3 on FL-HSC symmetric versus asymmetric differentiation and division. Here, E14.5 FL-HSCs were exposed to ANGPTL-3 in expansion media until their first cell division [42, 56]. Daughter cells were then replated in differentiation media. ANGPTL-3 did not affect the nature of the first cell division of FL-HSCs (Figure 4F). Thus, FL niche factors that expand adult BM-HSCs may not have the same effect on FL-HSCs.

FL-HSCs expand similarly to BM-HSCs in transplant recipients

Since our *in vitro* data suggest that FL-HSCs are prone to differentiation, we evaluated their self-renewal via serial transplantation. FL-HSCs outcompete adult BM-HSCs in competitive primary transplants [52]. Less is known about the competitive potential of FL-HSCs *versus* BM-HSCs in secondary repopulating assays [51, 57].

To test this, we transplanted CD45.2$^+$ E14.5 FL-HSCs (CD45.2$^+$ HSC^{FL}) and CD45.1$^+$ adult-BM-HSCs (CD45.1$^+$ HSC^{BM}) at a 1:1 ratio into lethally irradiated CD45.1$^+$/CD45.2$^+$ recipients (Figure 5A–B). As expected, FL-HSCs displayed a strong competitive advantage over BM-HSCs in primary recipients (FL-derived CD45.2$^+$ PB = 86%±4%, 20 weeks post-transplant) (Figure 5Bi), while CD45.2$^+$ BM-HSCs (CD45.2$^+$ HSC^{BM}) and CD45.1$^+$ HSC^{BM} displayed equivalent multilineage repopulating potential when competed against each other (Figure 5Bi).

Next, CD45.2$^+$ HSC^{FL} and CD45.1$^+$ HSC^{BM} were recovered from primary recipients and transplanted 1:1 into lethally irradiated CD45.1$^+$/CD45.2$^+$ secondary recipients (Figure 5A, 5Biii). Here, CD45.2$^+$HSC^{FL} no longer display a repopulating advantage over CD45.1$^+$HSC^{BM} (FL-derived CD45.2$^+$ PB = 35%±18% and BM-derived CD45.1$^+$ PB = 39%±20%, 16 weeks post-transplant, Figure 5Biii), revealing a loss of E14.5 FL-HSC competitive advantage upon secondary transplantation. Engraftment was multilineage in all cases. Interestingly, 16 weeks post-secondary transplantation FL-derived HSCs displayed higher lymphoid potential than adult BM-derived HSCs (Figure 5Biv).

To assess the frequency of FL and BM-derived HSCs in primary recipients, we performed limiting dilution transplantation assays (LDA) using CD45.2$^+$ HSC^{FL} and CD45.2$^+$ HSC$^{BM\text{-}HSC}$ from primary recipients. We found 1 in 37.9 (95% C.I.= 1/19.4 – 1/74.2) and 1 in 43.7 (95% C.I.= 1/23.5 – 1/81.2) competitive repopulating units (CRUs) in phenotypic CD45.2$^+$ HSC^{FL} and CD45.2$^+$ HSC$^{BM\text{-}HSC}$ isolated from primary recipients, respectively. Results fit the LDA model: p-value ≥ 0.71. Thus, phenotypic CD45.2$^+$ HSC^{FL} and CD45.2$^+$ HSC$^{BM\text{-}HSC}$ isolated from primary recipients contain the same number of transplantable HSCs (p-value=0.76, Figure 5C). As the frequency of RUs among primary transplanted FL-HSCs *versus* adult BM-HSCs is similar (1RU in 2.7 FL-HSCs [51], and 1RU in 2.5 adult HSCs [58–60]), our data suggest that the loss of competitive repopulating potential of FL-HSCs in secondary transplants does not result from an overall loss of FL-HSCs in primary recipients. Moreover, despite their cycling advantage relative to BM-HSCs when initially transplanted, FL-HSCs did not expand significantly in the BM of primary recipients, further supporting our *ex vivo* assays suggesting that cycling FL-HSCs do not favor symmetric divisions. This may result from a combination of FL-HSC cell-intrinsic programming and non-cell autonomous cues of the BM niche on transplanted FL-HSCs. However, FL and adult BM-HSCs removed from their niches and cultured *ex vivo* show differences in their expansion abilities, suggesting cell-intrinsic differences (Figure 4). Moreover, correcting for cell cycle differences, E16.5 FL-HSCs displayed an hscScore reminiscent of fetal and adult hematopoietic progenitor cells (HPCs, Lineage$^-$Sca-1$^+$c-Kit$^+$CD48$^+$), rather than adult BM-HSCs, confirming intrinsic transcriptional differences (p-value = 5.21×10^{-60}, Figure 6A–C)[61, 62]. These data further support our model that FL-HSCs are primed to differentiate.

Overall, our studies suggest that many FL-HSCs are biased towards differentiation, likely to support embryo's needs during development. This contributes to modest expansion of the pool of HSC progenitors that realize their potential to contribute to adult blood during the FL stage of hematopoietic ontogeny.

Discussion

The FL has classically been considered a niche supportive of HSC expansion due to the sharp increase in RUs during this stage [1, 8, 9, 12], a high percentage (25%) of cycling FL-HSCs, [10, 11, 13, 27] and the ability of FL-HSCs to outcompete BM-HSCs when transplanted [52]. This view assumes that most FL-HSCs divide symmetrically to expand the HSC pool. Here, we challenge this dogma by presenting evidence that HSCs fated for life-long hematopoiesis expand only modestly in the FL and that FL-HSCs are biased to differentiate or undergo asymmetric cell division.

Previous studies relied on transplantation of embryo-derived cells into conditioned recipients to estimate numbers of functional HSCs and progenitors [1–3, 8–14, 28]. However, this approach cannot detect cells too immature to repopulate recipients, though they may ultimately acquire this potential *in situ*. Likewise, each transplantable cell is not necessarily fated to contribute to adult haematopoiesis. Our non-invasive approach based on labelling blood progenitors at discrete stages of development [7, 28, 42] detected 848 and 1,032 endothelial progenitors contributing to HSCs and PB at P180, respectively (Figure 1Cii–D, Extended Data Figure 3B, Supplementary Table 1). By comparing the number of hematopoietic progenitors detected later in ontogeny to this baseline, the view of the dynamics of life-long blood progenitors across ontogeny significantly changes [28]. Remarkably, we observe only a ~two-fold increase in these progenitors between E10.5-P1 (Figure 1C–D, Supplementary Table 1). Consistently, the increase in RUs from E11.5 (1 RU) to E12.5 (60 RU) [1, 8, 9] was recently attributed to HSC progenitor maturation in the early FL [12], rather than proliferation, as previously assumed [1, 3, 8, 9, 63]. Thus, the FL likely serves as a site of pre-HSC maturation, rather than extensive HSC expansion. Further work is needed to assess if this maturation continues beyond E12.5.

Although our studies with a DOX-inducible *pTRE-H2BGFP* allele confirmed significant proliferation by phenotypic FL HSCs and their progenitors between E12.5-E14.5 (~four divisions, Figure 3D), this much expansion in every hemogenic endothelial progenitor fated to contribute to adult haematopoiesis (about 848) would yield roughly 14,000 HSCs by E14.5. This far exceeds both the number of transplantable E14.5 FL HSCs [1–3, 8–10] and our own *Confetti*-based estimates of life-long FL HSCs at P1 (about 1,800). Thus, although the phenotypic FL-HSC pool is clearly very proliferative [10, 11, 13, 27] (Figure 3), it is evident that many of these proliferations do not ultimately expand the HSC pool.

Rather, most phenotypic E14.5 FL HSCs appear biased for symmetric differentiation (57%) rather than symmetric division (only 6%) (Figure 4E). In contrast, fewer adult-BM-HSC symmetrically differentiate (24%) and more undergo symmetric divisions (26%) *in vitro* (Figure 4E). Moreover, when controlled for cell cycle status, FL-HSCs are transcriptionally most akin to adult and fetal MPPs, rather than adult-HSCs, supporting our model that many FL-HSC are primed for differentiation (Figure 6A–C). Many studies contribute to the classic view that FL HSCs symmetrically expand. Several report that many transplantable FL-HSCs have >2n DNA content [10, 13] and reside in S/G2/M [11]. As the frequency of FL-HSCs is stable from E12.5-E15.5 and the FL doubles in size each day [10, 55], the simplest explanation is that HSCs divide symmetrically, resulting in a dramatic increase in RUs [1, 2, 8–13, 15, 51, 52]. Importantly, only about 1/2.7 phenotypic E14.5 FL $CD150^{+}CD48^{-}Lin^{-}Sca\text{-}1^{+}c\text{-}Kit^{+}Mac\text{-}1^{+}$ HSCs are transplantable [51], revealing functional heterogeneity within the most stringently defined phenotypic FL HSCs[51]. Our data further reveal that most FL HSC cell divisions serve the hematopoietic needs of the embryo via differentiation with only modest expansion of life-long HSCs (Figures 4–5).

Although multiple proteins that support HSC are in the FL (e.g. ANGIOPOIETIN-3, EPO, SCF/KITL, CXCL12, ANGPTL3, among others[22, 27, 30–35]), none have been clinically translated to expand human HSCs *in vitro*, further suggesting that some may promote HSC maturation or survival, rather than expansion. Indeed, ANGPTL3 did not impact the

division of FL-HSC *ex vivo* (Figure 4F, Extended Data Figure 5B–E). Alternatively, these factors may support an environment that stochastically allows both HSC differentiation and expansion. They may also support expansion of the few HSCs that contribute to the adult HSC pool. Importantly, *ex vivo* HSC expansion is still an unmet clinical need[36–38]. Despite multiple drug screens, only a few molecules promote some HSC expansion (*e.g.* StemRegenin-1, UM171, and new culture conditions)[64, 65 27, 66 38]. This highlights the importance of focusing on the right developmental stage supportive of HSC expansion to identify expansion cues.

Placenta-derived transplantable HSCs also increase between E11.5-E12.5. Here, the placenta harbours 15-fold more HSCs than the AGM.[8] This RU expansion could derive from *de novo in situ* HSC specification, expansion of resident HSCs, or accumulation and expansion/maturation of AGM-derived HSCs circulating into the placenta via the umbilical arteries.[8, 15, 67] Thus, the placenta may constitute a maturation/expansion niche from which HSCs then migrate to the FL. In our unbiased approach, we measure the total contribution of HSC precursors to the adult HSC pool regardless of the embryonic site of origin or expansion. Further studies will be required to explore any role for the placenta in HSC expansion.

Our work also suggests that once HSCs move to the BM in significant numbers around birth, absolute numbers of HSCs progressively increase, as indicated by a 1.4- and 1.7-fold expansion between P9-P15 and P15-P21, respectively (Figure 1C–D, Supplementary Table 1). This expansion could be passively regulated by a growing BM niche that accommodates more HSCs, actively regulated by an evolving niche, or intrinsically programmed [68]. Notably, adolescence was also projected as the key window of human HSC expansion [41].

Intriguingly, the number of postnatal HSC-progenitors contributing to the adult HSC pool was less than that found to contribute to PB complexity at P60 and P180, suggesting the existence of HSPCs distinct from HSCs that contribute to PB for months into adult life. The numbers of progenitors contributing to BM HSPCs were also less than that seen in the PB (Figure 1Cii–D, Extended Data Figure 3B). Hence, the PB likely reflects the total output of multiple independent clonal pools. Our results support a model in which long-lived postnatal HSPCs contribute to PB for at least six months during homeostasis, in agreement with recent reports [48, 50, 69].

In sum, our data reveal that FL-HSCs are biased towards differentiation, rather than symmetric cell division, relative to phenotypic neonatal and adult bone marrow HSC. We propose that the HSC pool fated to contribute to life-long haematopoiesis expands only modestly during the FL stage of ontogeny. This work significantly alters our understanding of the role of the FL as an HSC niche and suggests that the FL might not be the appropriate place to look for HSC expansion cues.

Methods

Mice

All animal experiments were carried out according to procedures approved by the St Jude Children's Research Hospital Institutional Animal Care and Use Committee and comply with all relevant ethical regulations regarding animal research. Here, animals are subject to an automated 12 hour on, 12 hour off light cycle. During the off light cycle, the red lights can be used to access animal room. Each animal room has a separate thermostat and humidistat to control temperature and humidity at the room level. Temperature and humidity are continuously monitored and alarms alert personnel to excursions from defined temperature or humidity ranges. C57BL/6J, C57BL/6.SJL-PtprcaPep3b/BoyJ, *ROSA26*$^{+/\text{Confetti}}$ (*Gt(ROSA)26Sor*$^{tm1(CAG-Brainbow2.1)Cle}$/J) (#013731), *ROSA26*$^{rtTa/rtTA}$ (B6.Cg-*Gt(ROSA)26Sor*$^{tm1(rtTA*M2)Jae}$/J (stock #006965), *Col1a1*$^{tetO\text{-}H2B\text{-}GFP/+}$ (*Col1a1*$^{tm7(tetO\text{-}HIST1H2BJ/GFP)Jae}$*/J)* (stock #016836), *pTRE-H2BGFP*$^{+/GFP}$ (Tg(tetO-HIST1H2BJ/GFP)47Efu/J (stock #005104), Ubiquitin$^{+/\text{ERT2-Cre}}$ (B6.Cg-Ndor1Tg(UBC-cre/ERT2)1Ejb/1J (stock #007001), VE-cadherin-Cre$^{+/T}$ mice (B6.FVB-Tg(Cdh5-cre)7Mlia/J (stock #006137)), FVB/NJ (stock #001800) mice were used (Jackson Laboratory (Bar Harbor, Maine) and housed in a pathogen-free facility.

Cell lines

Inducible *ROSA26*$^{rtTA/rtTA}$*; pTRE-H2BGFP*$^{+/GFP}$ *(TRE-H2B-GFP)* immortalized mouse embryonic fibroblasts (MEFs) were derived from E13.5 embryos in our own laboratory. Genotypes were obtained post-isolation by Polymerase chain reactions (PCRs) as detailed in the genotyping section at the time of isolation. Sex of the embryos is unknown.

Genotyping

PCRs were performed employing Go Taq DNA Polymerase (Promega) following manufacturer's instructions. PCR conditions: (95°C, 2'); ((94°C, 30"; 56°C, 30"; 72°C, 30"] × 35); (72°C, 10'). Primers: Cre F1 (5'-CTGTTACGTATAGCCGAAAT-3'), Cre R1 (5'-CTACA CCAGAGACGGAAATC T-3'). CRE-positive PCR band: 203 bp. Detection of the GFP allele was used for *Confetti*, *Col1a1*$^{tetO\text{-}H2B\text{-}GFP}$ and *pTRE-H2BGFP*^{GFP} alleles genotyping: GFP Fw (5'-CAGATGAAGCAGCACGACTTCT-3'), GFP Rv (5'-AACTCCAGCAGGACCATGTGAT-3'). GFP PCR band: 400 bp. To detect the *ROSA26*^{rtTa} allele we employed the following primers obtained from Jackson laboratories: oIMR8052 (mutant reverse) (5'- GCG AAG AGT TTG TCC TCA ACC −3'), oIMR8545 (mutant reverse) (5'- AAA GTC GCT CTG AGT TGT TAT −3'), oIMR8546 (mutant reverse) (5'-GGA GCG GGA GAA ATG GAT ATG −3'), WT band (650bp), Mutant band (340bp).

Transplants

CD45.2^{+} HSC were sorted from E14.5 FL or from P60 adult BM cells from C57BL/6J mice and co-transplanted with CD45.1^{+} HSC sorted from P60 adult BM cells from C57BL/6.SJL-PtprcaPep3b/BoyJ mice in a 1:1 ratio as 280 CD45.2^{+} HSCs *vs* 280 CD45.2^{+} HSCs were transplanted via tail vein injection into 8-12 week old CD45.2^{+}/CD45.1^{+} C57BL/6J mice previously subjected to 11 Gy of ionizing radiation in split doses of 5.5

Gy. For secondary transplants, CD45.2$^+$ HSCs were sorted from mice primary transplanted with CD45.2$^+$ E14.5 FL-HSC (CD45.2$^+$HSC^{FL}); and CD45.1$^+$ HSC (CD45.1$^+$HSC^{BM}) were sorted from mice primary transplanted with both CD45.1$^+$ and CD45.2$^+$ adult-HSC recipient mice. CD45.2$^+$HSC^{FL} and CD45.1$^+$HSC^{BM} were competitively transplanted into congenic CD45.2$^+$/CD45.1$^+$ C57BL/6J recipients. For limiting dilution assays from primary transplanted recipients, we sorted CD45.2$^+$HSC^{FL} or CD45.2$^+$HSC^{BM} from the primary recipients and transplanted 20, 60, 180 or 500 together with a radioprotective dose of 200,000 CD45.1$^+$ WBM cells into lethally irradiated CD45.2$^+$/CD45.1$^+$ C57BL/6J secondary recipients.

Differentiation potential assay

Single HSCs were sorted into 96-well non-tissue-culture-treated U-bottom plates (Corning, NY, USA) and cultured for 14 days in 200μl of medium supportive of erythro-myeloid differentiation [*i.e.* differentiation media: Prime XV Mouse hematopoietic Cell medium, Irvine Scientific) supplemented with 50 μM 2-mercaptoethanol (Sigma-Aldrich, St. Louis, MO), 2 mM L-glutamine (Invitrogen, Carlsbad, CA), 100 units/ml penicillin (Invitrogen), 100 μg/ml streptomycin (Invitrogen), 20 ng/ml mouse Stem cell factor (PeproTech, Rocky Hill, NJ), 20 ng/ml mouse Thrombopoietin (PeproTech), 20 ng/ml mouse Interleukin-3 (Cat # 213-13 PeproTech), 5 units/ml human Erythropoietin (EPOGEN® Amgen, Thousand Oaks, CA), and 10% heat-inactivated fetal bovine serum (Invitrogen)][42, 70]. Emerging colonies were harvested, stained with May-Grünwald (Sigma-Aldrich) and Giemsa stain (Sigma-Aldrich), mounted employing Cytoseal™ Mounting Medium (Richard-Allan Scientific, Thermo Fisher Scientific, Waltham, MA) and analyzed for erythro-myeloid lineages including: granulocytes, monocytes, erythrocytes and megakaryocytes[42].

Paired daughter cell assays

Single HSCs were sorted into 384-well plates with 25 μl of expansion media containing Stemspan medium (StemCell Technologies, Vancouver, British Columbia, Canada) supplemented with mSCF and mTPO (each at 100 ng/ml; Cat # 250-03 and 315-14 Peprotech)[56].

About 24 hours later wells were visually inspected for the presence of two cells. When two cells were detected, each daughter cell was plated into a new well (on a 96 well-plate) containing 200ul of differentiation media keeping track of paired-daughters. Daughter cells were cultured for 14 additional days. Then, emerging colonies were processed as indicated above.

PB Analysis

PB was obtained from the retro-orbital plexus using heparinized capillary tubes (#22-362566 Fisherbrand) and lysed in red blood cell lysis buffer (R7757, Sigma-Aldrich)[7] employing the following antibodies: CD45.1-APC (A20) (Biolegend, San Diego, CA); B220-PECy7 and CD8-PECy7 (53-6.7) (Tonbo Biosciences, San Diego, CA); CD45.2-V500 (104), B220-PerCPCy5.5 (RA3-6B2), Gr1-PerCPCy5.5 (RB6-8C5), CD11b-PerCPCy5.5 (M1/70) and CD4-PECy7 (RM4-5) (BD Biosciences, San Diego, CA) and Ter119-PECy7 (TER-119)

(Biolegend). Dilutions used and catalogue identifiers for each antibody are provided in Supplementary Table 2.

Bone Marrow and Fetal Liver Analysis

Bone marrow was harvested from the femurs, tibias, and pelvic bones of mice by crushing. c-Kit$^+$ cells were enriched using anti-c-Kit microbeads (Cat #130-091-224, Miltenyi Biotech, San Diego, CA) followed by magnetic separation (autoMACS Pro Separator; Miltenyi Biotech). Previously enriched c-Kit$^+$ cells were incubated with a cocktail of biotin-conjugated monoclonal antibodies against CD5, CD11b, B220, 7-4, Gr-1, and Ter-119 (Cat. No. 130-090-858, Miltenyi Biotech). Enriched c-Kit$^+$ cells were stained with antibodies to define HSPC populations as follows[42]: HSC [Streptavidin-BV605 (Biolegend), Sca-1-PerCP-Cy5.5 (E13-161.7) (Biolegend), c-Kit-APC-780 (2B8) (Thermo Fisher Scientific, Waltham, MA), CD48-APC (HM48-1) (Biolegend), CD150-PE-Cy7 (TC15-12F12.2) (Biolegend)]; MPPs/CLPs [Streptavidin-BV605, Sca-1-PerCP-Cy5.5, c-Kit-APC-780, CD135-APC (A2510) (Biolegend), CD127-PECy7 (A7R34) (Tonbo Biosciences)]; CMPs/GMPs/MEPs (Streptavidin-BV605, Sca-1-PerCP-Cy5.5, c-Kit-APC-780, CD32/16-PECy7 (93) (Biolegend), CD34-A647(RAM34) (BD Biosciences)]. Dilutions used and catalogue identifiers for each antibody are provided in Supplementary Table 2. 4',6-diamidino-2-phenylindole (DAPI) was used to exclude dead cells. Cells were analyzed on a FACSAria III (BD Biosciences, San Diego, CA) and FlowJo20 version 9.4.11 (Tree Star, Ashland, OR) was used to analyse related data.

Tamoxifen delivery in vivo

To activate CRE in utero during E12.5-E15.5, pregnant females were treated for 3 consecutive days (E12.5-E14.5) by oral gavage with 2mg of tamoxifen (TAM, T5648, Sigma-Aldrich) suspended in 90% sunflower seed oil (Sigma-Aldrich) and 10% ethanol (Pharmco-AAPER). Mice were always treated around noon, with 200ul of a 10mg/ml TAM. Caesarean section was performed on day E19 in any mother showing any issue on delivering pups. Pups were then fostered with FVB mothers.

To activate CRE at P1, pups were treated with a single intraperitoneal injection of 50ul of TAM 5mg/ml (*i.e.* 0.25 mg TAM; 150mg TAM/kg body weight).

To activate CRE at P8-P10, pups were intraperitoneally injected for two consecutive days with 75ul of TAM 5mg/ml (at P8 and P9) (*i.e.* 0.375 mg of TAM; 75 mg TAM/kg body weight).

To activate CRE at P14-P16, pups were intraperitoneally injected for two consecutive days with 75ul of TAM 5mg/ml (at P14 and P15) (*i.e.* 0.375 mg of TAM; 50 mg TAM/kg body weight).

To activate CRE at P21-P23, pups were intraperitoneally injected for two consecutive days with 100ul of TAM 5mg/ml (at P21 and P22) (*i.e.* 0.5 mg of TAM; 50mg TAM/kg body weight).

Doxycycline delivery in vivo

To activate rtTa *in utero*, timed pregnancies were set up and females showing a vaginal plug were treated with DOX in the drinking water (1 mg/mL of DOX + 10% sucrose) from day 0.5 post-coitum (0.5 dpc) to 3.5 dpc. Starting on 4.5 dpc, females were injected intravenously with a DOX solution four or five times every other day as 25 ug of DOX/g of body weight (*i.e.* 50 uL of a 10mg/mL DOX solution for a 20g mouse). DOX [Doxycycline Hyclate D9891 (Sigma)] solution was prepared in PBS and filtered with a 0.22um filter. To activate rtTa until day E12.5, females were treated four times, last injection being on day E11.5. To maintain rtTa activated until day E14.5, females were injected for a fifth time on day E13.5.

To determine the in vivo window of DOX activity

To estimate the window of DOX activity in vivo, 5×10^6 WBM cells from *ROSA26* $^{rtTa/+}$ *Col1a1* $^{tetO\text{-}H2B\text{-}GFP/+}$ *CD45.2* $^{+}$ pooled BM isolated from three *ROSA26* $^{rtTa/+}$ *Col1a1* $^{tetO\text{-}H2B\text{-}GFP/+}$ *CD45.2* $^{+}$ mice was transplanted into CD45.1$^+$/CD45.2$^+$ congenic recipients treated with DOX three days (day −3), two days (day −2) or one (day −1) day prior to transplant or on the day of transplant (day 0). Recipient mice were treated with a single intravenous injection of DOX (25 ug of DOX/g of body weight, *i.e.* 50 uL of a 10mg/mL DOX solution for a 20g mouse). DOX solution was prepared in PBS and filtered with a 0.22um filter.

Doxycycline delivery in vitro

To activate rtTa *in vitro*, DOX was administered as 100ng/ml.

Derivation and culture of inducible ROSA26$^{rtTA/rtTA}$;pTRE-H2BGFP$^{+/GFP}$ (TRE-H2B-GFP) cells.

Mouse embryonic fibroblasts (MEFs) were isolated from E13.5 embryos propagated and immortalized according to standard protocols [71]. MEFs were cultured in Dulbecco's minimal essential medium (DMEM, Thermo Fisher Scientific) with 10% fetal calf serum (FCS, Omega Scientific).

ROSA26$^{rtTa/rtTA}$; pTRE-H2BGFP$^{+/GFP}$ system to study cell division

After three days in DOX (a time when ≥99% of the cells are GFP$^+$) DOX was removed and cells cultured thereafter without DOX (Pulsed). Every three days cells were analyzed by flow cytometry and manually counted to calculate the number of divisions and 1×10^6 cells were plated back in a 10cm tissue culture plate.

Flow cytometry analysis

Analyses were performed on a BD FACSAria III SORP (Special Order Research Product) or LSR Fortessa (both BD Biosciences, San Diego, CA) and the data analyzed with FlowJo version 9.4.11 (Tree Star, Ashland, OR).

Statistics & Reproducibility

No randomization method was used. No statistical method was used to predetermine sample size, but our sample sizes are similar to those reported in previous publications[7, 42]. Animals were allocated into experimental groups according to genotype. Although no specific methods were used for blinding, blood and bone marrow samples were collected from mice by one individual and then analysed by flow cytometry by a different individual, at which time genotypes/treatment were not known. All statistics were performed by an independent biostatistics experts who were unaware of the biological significance of distinct groups of mice being examined. GFP^+ were excluded from *Confetti*-related analyses, because as we previously described the $\%GFP^+$ cells always fell below the minimum threshold for precision[7, 42].

Experiments were reliably reproduced. Major findings, which include that the pool of fated progenitors expands only two-fold during FL ontogeny, we observed similar results supporting these conclusions in different haematopoietic compartments including PB and HSCs and at different ages (P60 and P180 in the PB). Our results in Histone2B-GFP retention *in vivo* experiments confirmed significant proliferation of phenotypic FL-HSC between E12.5 and E14.5, and we obtained consistent results in paired daughter-cell assays in several independent experiments both with and without ANGPTL3 supporting that many mid-gestation phenotypic FL-HSC are biased to differentiate, rather than self-renew.

Statistics and use of formula for predicting cell number from sample-to-sample variance.

Summary statistics, including mean and standard deviation were indicated. To calculate the clonal complexity of any tissue at any given time point, we used the mouse-to-mouse variance in *Confetti* color distribution [7]. The 95% confidence intervals were provided.

In all cases, *Confetti*-based estimates of precursor numbers were normalized to labelling efficiency, as previously described [total initiating events = estimate × (100/percentage of $Confetti^+$ cells)][7, 42]. In all the conditions, labelling efficiency exceeded >10%. *Confetti*-based estimates of numbers of initiating events maintain fidelity when labelling efficiency is >3% and >500 cells are examined[7].

The normality of the data was tested by use of Shapiro-Wilk test. Analysis of variance (ANOVA) or Kruskal-Wallis test was then used to compare more than two groups. Depending on these, two-sample t or exact Wilcoxon rank sum test was used to compare two groups. The efficiency of *Confetti*-labeling was assessed for every cohort of mice examined (Extended Data Figure 2, Supplementary Table 1) and used to correct the estimates of the total numbers of blood progenitor to account for both the labeled and unlabeled fractions, as previously described [7, 42]. *Confetti*-labelling efficiencies ranged from 9% to 60% (Extended Data Figure 2, Supplementary Table 1). Multivariate analysis of variance was also used to compare more than two groups by different conditions. The relationship between the estimated number of divisions and the actual number of divisions was examined using diagnosis plots and the cook's distance. False discovery rate (FDR) method developed by Benjamini & Hochberg [72] was used to adjust for multiple testing corrections at a level

of 0.05. Otherwise, p-values <0.05 were considered statistically significant. Analyses were conducted in R-3.5.3.

Single cell transcriptomics

Single cell transcriptional profiles of E16.5 FL-HPCs (Lineage$^-$Sca-1$^+$c-Kit$^+$CD48$^+$) were integrated with E16.5 FL HSCs (GSE128761)[68] using Seurat (v3.2.2). Each data set was processed separately to define quality cells (nFeature_RNA > 200 & nFeature_RNA < 6000 and percent mitochondrial < 5). Variable features (n=2000) were defined using the vst selection method. A cell cycle variable was defined and regressed using standard Seurat methods. Marker genes were identified between E16.5 FL HPCs and E16.5 FL HSCs using a log2FC threshold > 0.25 and min.pct = 0.25. Similar analyses were performed for adult HPCs and adult HSCs. Pairwise comparisons of significant marker genes (p_val_adj < 0.05) were calculated and displayed in venn diagrams.

hscScore

Single cell transcriptional profiling of E16.5 FL and adult HPCs and HSCs (GSE128761) were scored via hscScore, as described previously[61, 62, 68]. This model uses Multi-Layer Perceptron (MLP), a machine learning algorithm that assigns a score representing how likely a cell is to be a true HSC. The scores are then interpolated between 0 and 1. Wilcoxon rank sum test was performed comparing HSC score distributions of E16.5 FL HSC and adult HSCs.

Critical reagents—A list for critical reagents including antibodies, key chemicals, cell lines, experimental models, oligonucleotides, softwares is provided in Supplementary Table 2.

Data availability—Source data for Supplementary Table 1, Figs. 1C–D, 2D, 3C–D, 4B, 4E, 4Fii, 5B, 5C, 6A–B, and Extended Data Figures. 2, 3, 4B–C and 5D–E are provided in Source Data Figures 1–6, Source Data ED Figures 2–5 and Source Data Supplementary Table 1. Previously published E16.5 FL HSC and adult HSC data that were re-analysed here are available in the Gene Expression Omnibus (GEO) under accession code GSE128761. All other data supporting the findings of this study are available from the corresponding author on reasonable request.

Materials availability—All unique reagents generated in this study (*i.e.* pTRE-H2B-GFP immortalized cell lines) are available with a completed Materials Transfer Agreement.

Extended Data

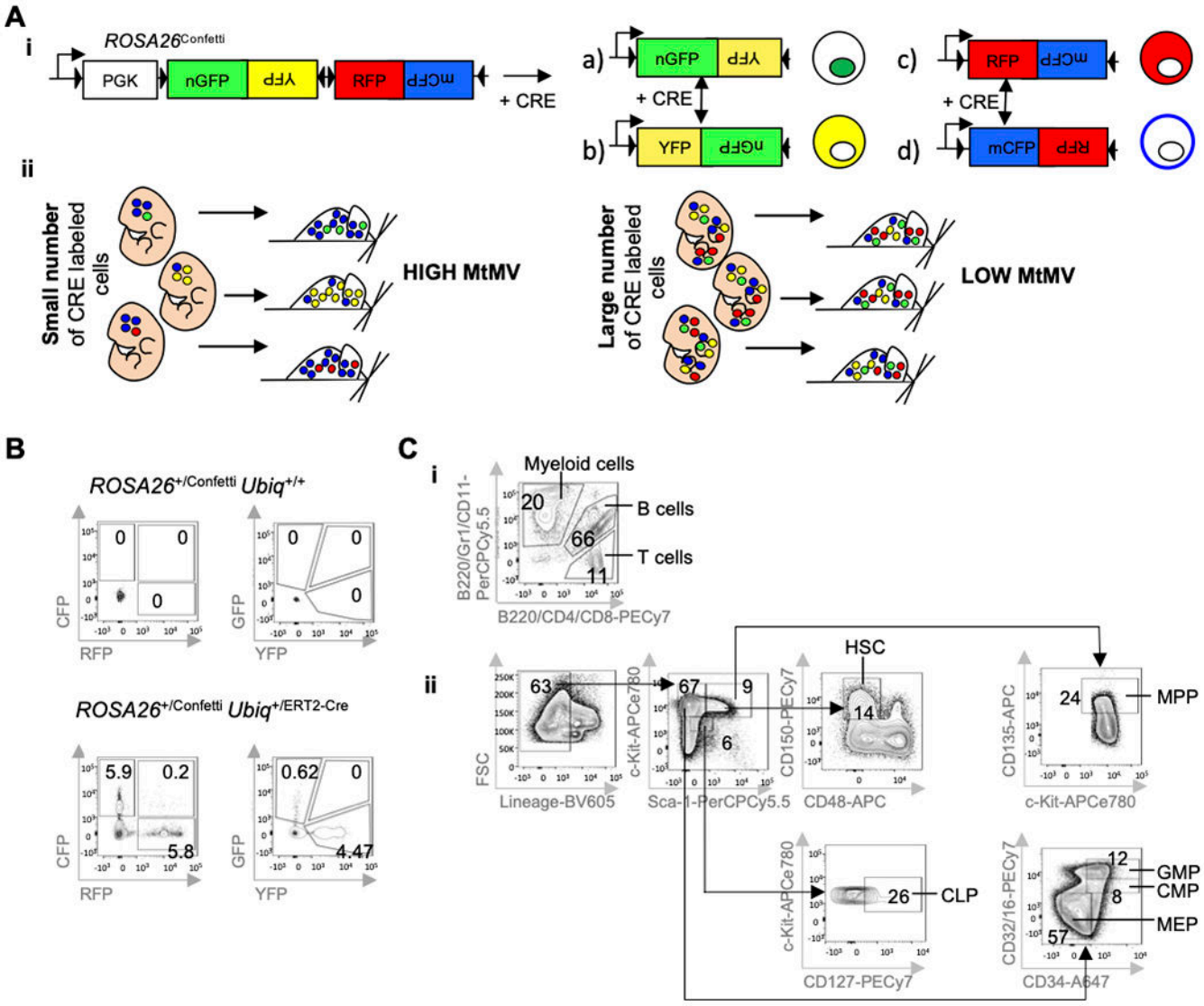

Extended Data Fig. 1. Schematic of *Confetti*-allele based approach to estimate clonal complexity, flow cytometry gating and summary of *Confetti* labelling in blood and bone marrow.

A. *Confetti*-allele approach to estimate cell numbers. **Ai.** Schematic of *Confetti* allele. **Aii.** Mouse-to-Mouse Variance in the distribution of *Confetti* colors (MtMV) inversely correlates with the number of initiating events. **B.** Representative *Confetti* gating. B-cells from a TAM-treated $ROSA26^{+/Confetti}Ubiq^{+/ERT2\text{-}Cre}$ mouse and a $ROSA26^{+/Confetti}Ubiq^{+/+}$ negative control are shown. **C.** Flow cytometry gating strategy of PB. (**Ci**) B-cells (B), T-cells (T) and myeloid cells (M), as well as BM compartments (**Cii**).

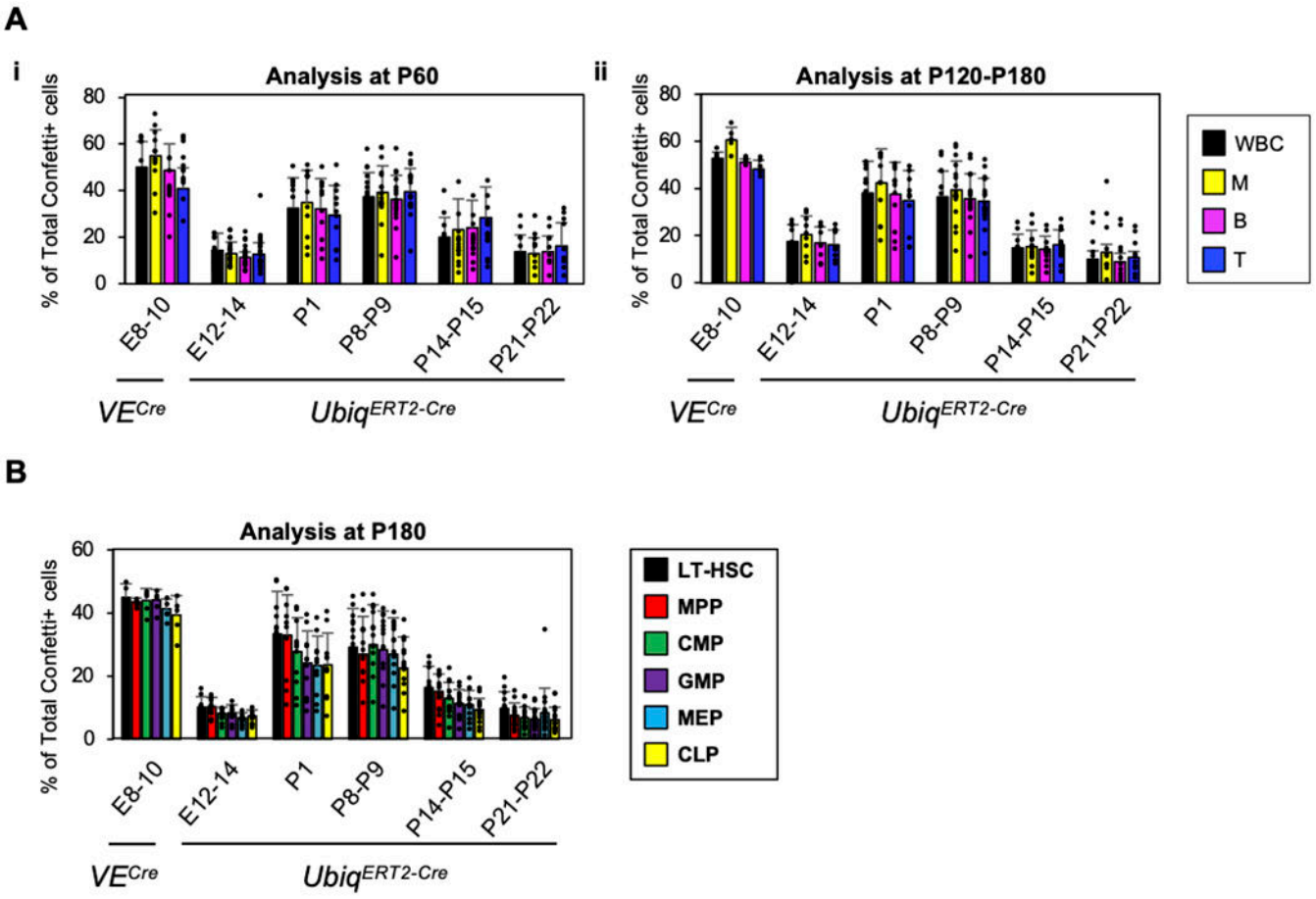

Extended Data Fig. 2. Summary of *Confetti* labelling in blood and bone marrow.

A. Average total PB *Confetti* label of mice at **(Ai)** two (n≥8: E8-10, n=16; E12-14, n=18; P1, n=11; P8-9, n=18; P14-15, n=13; P21-22, n=8) and **(Aii)** six months of age (n≥4: E8-10, n=5; E12-14, n=9; P1, n=11; P8-9, n=18; P14-15, n=13; P21-22, n=4). **B.** Average total *Confetti* labeling in the BM at six months of age (n≥4: E8-10, n=5; E12-14, n=9; P1, n=11; P8-9, n=18; P14-15, n=13; P21-22, n=4). **A-B.** Related to Figure 1C–D and Extended Data Figure 3. **A-B.** Means are shown. Error bars indicate standard deviation. Individual data points are shown in black.

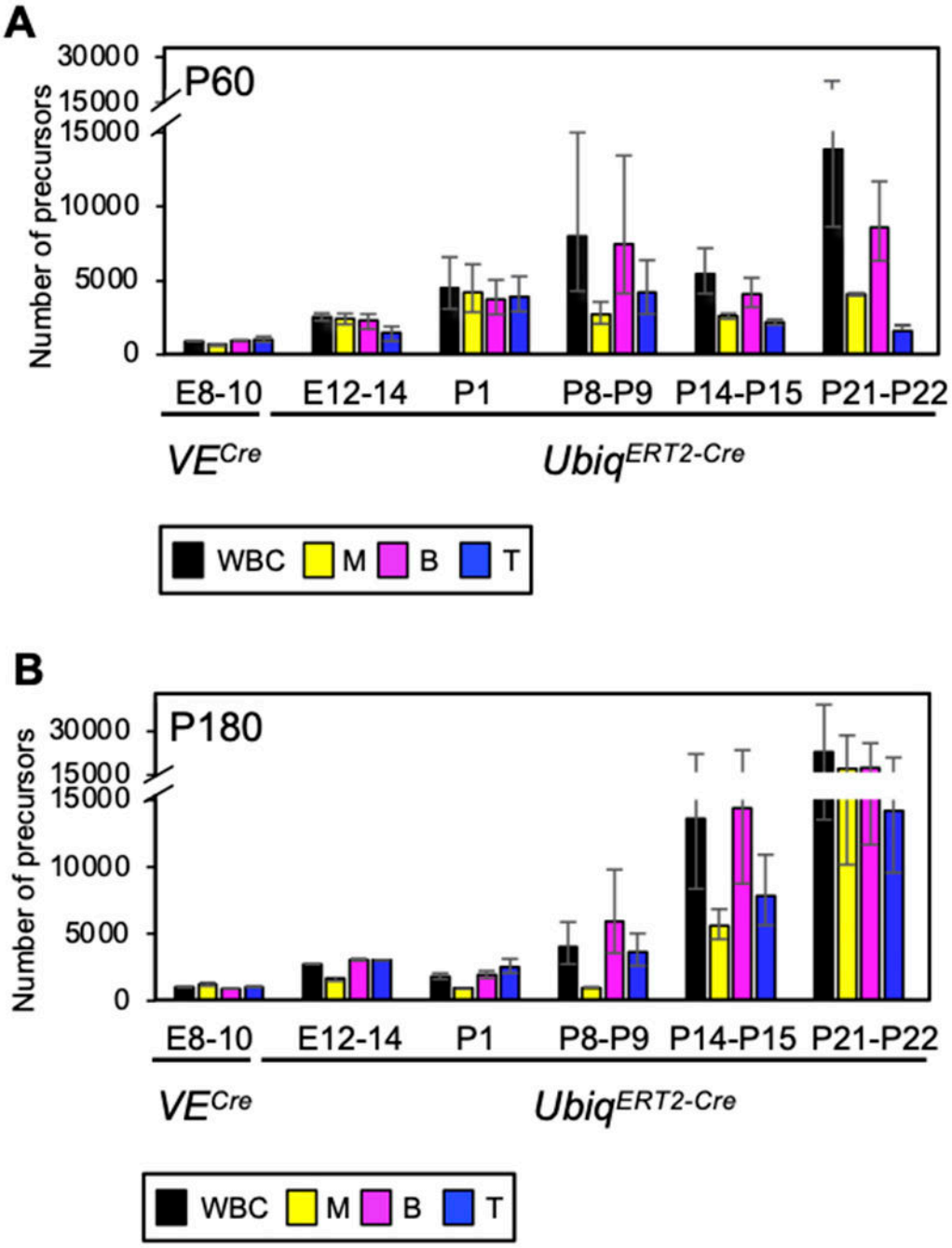

Extended Data Fig. 3. Numbers of fetal liver hematopoietic progenitors contributing to specific adult blood compartments.

MtMV-based estimates of numbers of progenitors contributing to PB at P60 (n≥8: E8-10, n=16; E12-14, n=18; P1, n=11; P8-9, n=18; P14-15, n=13; P21-22, n=8) (A) and P180 (n≥4: E8-10, n=5; E12-14, n=9; P1, n=11; P8-9, n=18; P14-15, n=13; P21-22, n=4) (**B)** labeled at distinct windows of ontogeny are shown. Total white blood cells (WBC), B-cells (B), T-cells (T) and myeloid cells (M). Related to Figure 1C. Error bars indicate the 95% confidence intervals.

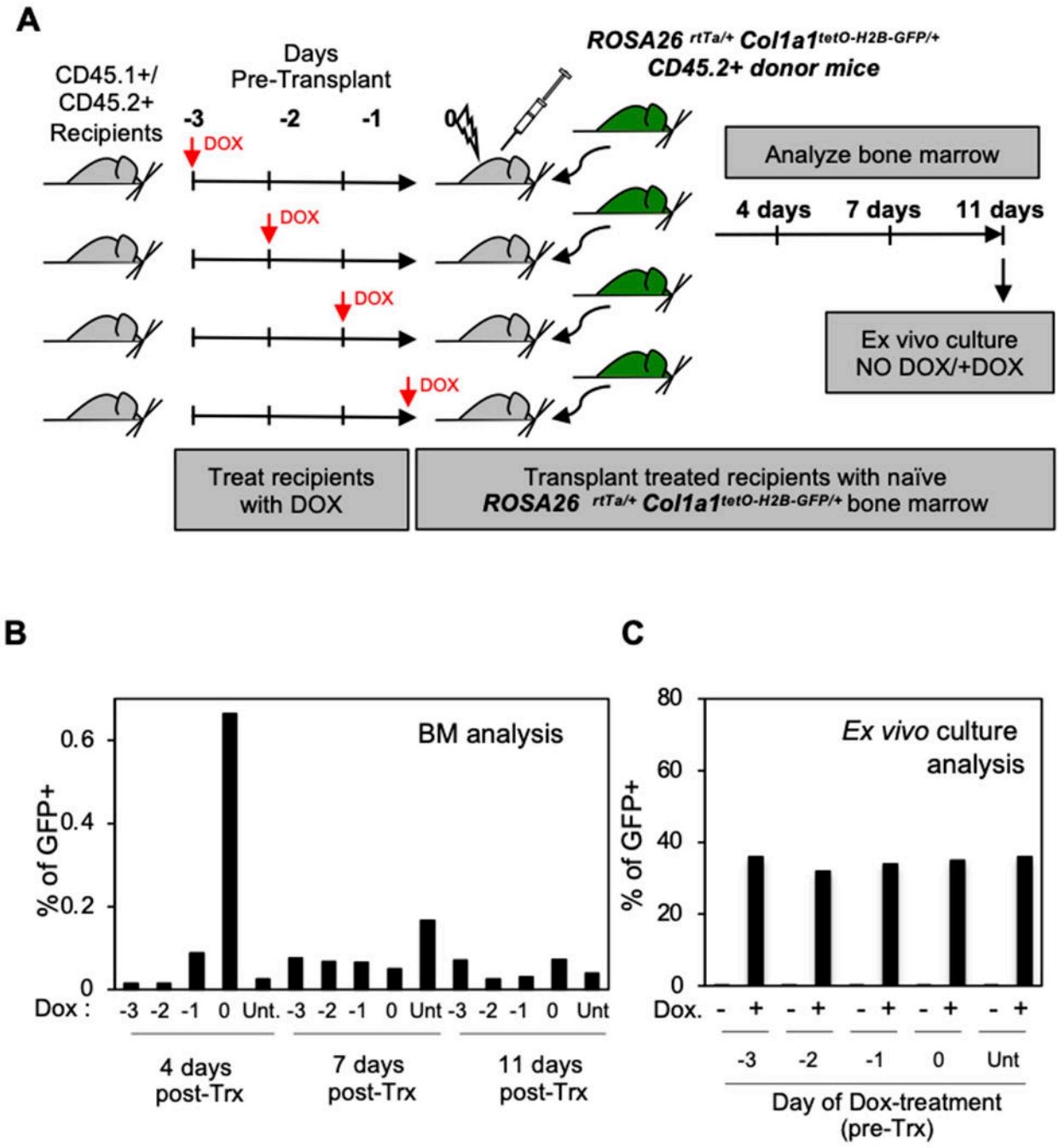

Extended Data Fig. 4. Window of active labelling of DOX *in vivo*.

A. Experimental schematic. *ROSA26* $^{rtTa/+}$ *Col1a1*$^{tetO\text{-}H2B\text{-}GFP/+}$ CD45.2^{+} donor BM [68] was pooled from five donors and transplanted into CD45.1^{+}/CD45.2^{+} recipient mice previously treated with DOX on day three (−3), two (−2) or one (−1) before transplantation or on the same of transplant (day 0) (n=3 recipients per group). **B.** %GFP^{+} BM of recipients 4, 7, or 11 days post-transplant (Trx). **C.** To corroborate the ability of non-labelled transplanted CD45.2^{+} cells to respond to DOX, CD45.2^{+} c-Kit^{+} sorted cells from each mouse cohort

were cultured *in vitro* in the presence or absence of DOX showing that cells were responsive to DOX *in vitro*.

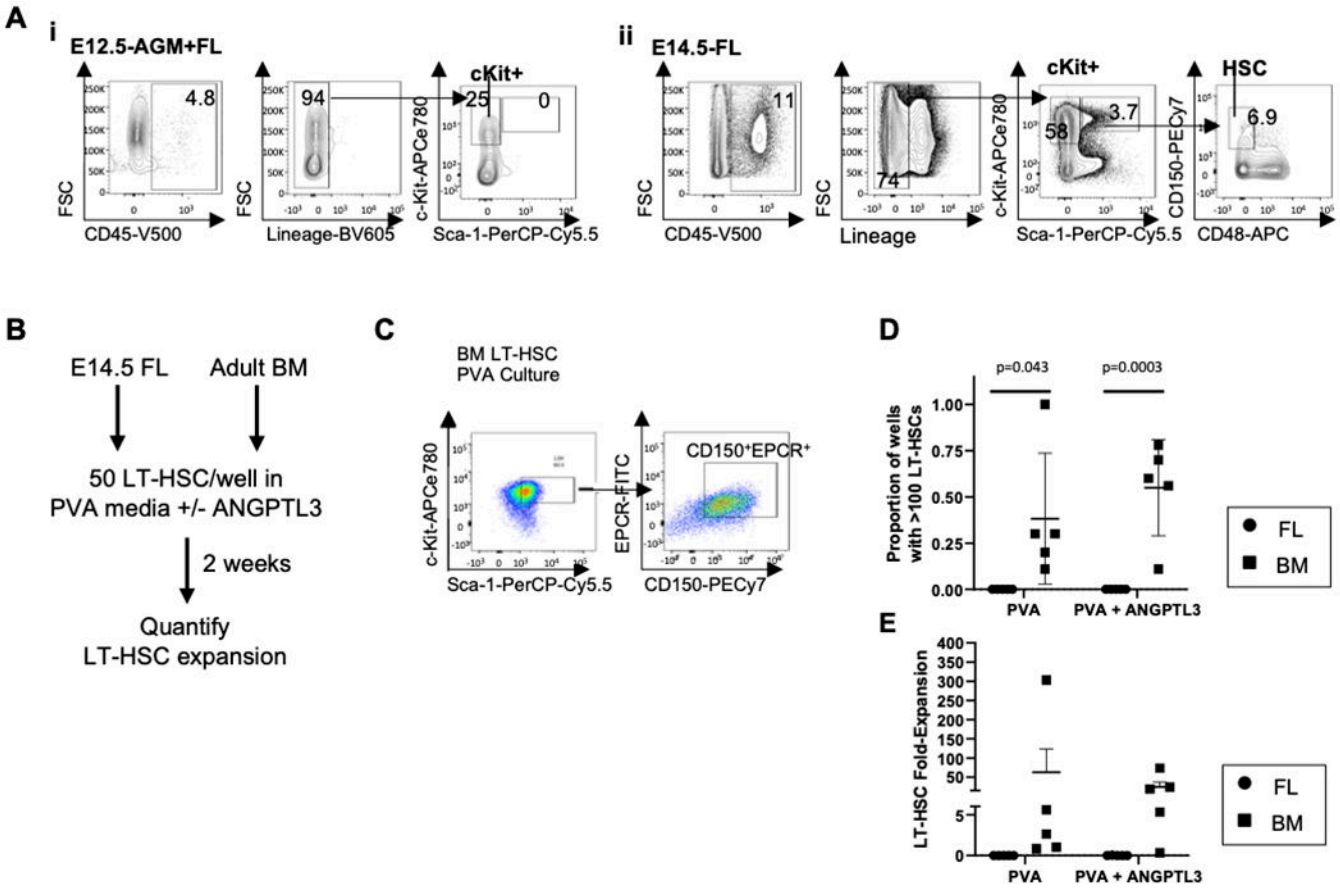

Extended Data Fig. 5. Fetal liver factor ANGPTL3 is not able to promote self-renewing expansion of E14.5 FL-HSCs.

A. Gating strategy on E12.5-CD45$^+$c-Kit$^+$ cells and E14.5-c-Kit$^+$ and E14.5-HSC cells. Related to Figures 3B–C & 4. **B-D.** LSK CD150$^+$CD48$^-$ C57Bl/6 HSCs were isolated from E14.5 FL or adult BM and cultured in PVA cultures tailored for self-renewing expansion either with or without addition of ANGPTL3, for 2 weeks. Immunophenotypic HSC expansion was then quantified. Due to known immunophenotypic shifts during PVA culture, HSC were defined as LSK CD150$^+$EPCR$^+$ after culture. **B.** Experimental schematic. **C.** Gating strategy of LSK CD150$^+$EPCR$^+$ HSC after culture. **D.** Proportion of wells expanding, defined as containing at least 100 immunophenotypic LT-HSCs. **E.** For those wells showing cell expansion, HSC expansion as a ratio of output/input is shown. For each condition, 5 biological replicates and 2 independent experiments with 10 wells/replicate. Each circle/square represents an individual biological replicate. Means and standard deviations are depicted. For (D), the Holm-Sidak method (2-tailed) was used to calculate statistical significance and correct for multiple comparisons. Exact p-values are shown in Figure.

Supplementary Material

Refer to Web version on PubMed Central for supplementary material.

Acknowledgements

We thank W. Clements, the McKinney-Freeman laboratory and Department of Hematology at St. Jude Children's Research Hospital (St. Jude) for critical discussions and reading of the manuscript; D. Ashmun, S. Schwemberger, and J. Laxton for FACS support; C. Davis-Goodrum, K. Millican, A. Reap, and C. Savage for help with transplants. This work was supported by the American Society of Hematology (S.M.-F.), the Hartwell Foundation (S.M.-F.), the NIDDK (K01DK080846 and R01DK104028, S.M.-F.), the American Lebanese Syrian Associated Charities (ALSAC) (S.M.-F.). M.G. is funded by the American Society of Hematology (Global Research Award), Barts Charity, Leukaemia UK (John Goldman Fellowship, 2020/JGF/001) and Medical Research Council (MRC Career Development Award, MR/V009222/1). E.A.O is supported by an Edward P. Evans Foundation Discovery Research Grant, an American Society of Hematology Scholar Award, and a Gabrielle's Angel Foundation Medical Research Award. The content is solely the responsibility of the authors and does not necessarily represent the official views of the National Institutes of Health.

References

1. Kumaravelu P et al. Quantitative developmental anatomy of definitive haematopoietic stem cells/long-term repopulating units (HSC/RUs): role of the aorta-gonad-mesonephros (AGM) region and the yolk sac in colonisation of the mouse embryonic liver. Development 129, 4891–4899 (2002). [PubMed: 12397098]
2. Medvinsky A & Dzierzak E Definitive hematopoiesis is autonomously initiated by the AGM region. Cell 86, 897–906 (1996). [PubMed: 8808625]
3. Muller AM, Medvinsky A, Strouboulis J, Grosveld F & Dzierzak E Development of hematopoietic stem cell activity in the mouse embryo. Immunity 1, 291–301 (1994). [PubMed: 7889417]
4. North T et al. Cbfa2 is required for the formation of intra-aortic hematopoietic clusters. Development 126, 2563–2575 (1999). [PubMed: 10226014]
5. Yokomizo T et al. Requirement of Runx1/AML1/PEBP2alphaB for the generation of haematopoietic cells from endothelial cells. Genes Cells 6, 13–23 (2001). [PubMed: 11168593]
6. Boisset JC et al. Progressive maturation toward hematopoietic stem cells in the mouse embryo aorta. Blood 125, 465–469 (2015). [PubMed: 25301706]
7. Ganuza M et al. Lifelong haematopoiesis is established by hundreds of precursors throughout mammalian ontogeny. Nat Cell Biol 19, 1153–1163 (2017). [PubMed: 28920953]
8. Gekas C, Dieterlen-Lievre F, Orkin SH & Mikkola HK The placenta is a niche for hematopoietic stem cells. Dev Cell 8, 365–375 (2005). [PubMed: 15737932]
9. Ema H & Nakauchi H Expansion of hematopoietic stem cells in the developing liver of a mouse embryo. Blood 95, 2284–2288 (2000). [PubMed: 10733497]
10. Morrison SJ, Hemmati HD, Wandycz AM & Weissman IL The purification and characterization of fetal liver hematopoietic stem cells. Proc Natl Acad Sci U S A 92, 10302–10306 (1995). [PubMed: 7479772]
11. Batsivari A et al. Understanding Hematopoietic Stem Cell Development through Functional Correlation of Their Proliferative Status with the Intra-aortic Cluster Architecture. Stem Cell Reports 8, 1549–1562 (2017). [PubMed: 28479304]
12. Rybtsov S, Ivanovs A, Zhao S & Medvinsky A Concealed expansion of immature precursors underpins acute burst of adult HSC activity in foetal liver. Development 143, 1284–1289 (2016). [PubMed: 27095492]
13. Fleming WH et al. Functional heterogeneity is associated with the cell cycle status of murine hematopoietic stem cells. J Cell Biol 122, 897–902 (1993). [PubMed: 8349737]
14. Medvinsky A, Rybtsov S & Taoudi S Embryonic origin of the adult hematopoietic system: advances and questions. Development 138, 1017–1031 (2011). [PubMed: 21343360]
15. Mikkola HK & Orkin SH The journey of developing hematopoietic stem cells. Development 133, 3733–3744 (2006). [PubMed: 16968814]

16. Bowie MB et al. Hematopoietic stem cells proliferate until after birth and show a reversible phase-specific engraftment defect. J Clin Invest 116, 2808–2816 (2006). [PubMed: 17016561]
17. Lessard J, Faubert A & Sauvageau G Genetic programs regulating HSC specification, maintenance and expansion. Oncogene 23, 7199–7209 (2004). [PubMed: 15378080]
18. Benz C et al. Hematopoietic stem cell subtypes expand differentially during development and display distinct lymphopoietic programs. Cell Stem Cell 10, 273–283 (2012). [PubMed: 22385655]
19. Qian H et al. Distinct roles of integrins alpha6 and alpha4 in homing of fetal liver hematopoietic stem and progenitor cells. Blood 110, 2399–2407 (2007). [PubMed: 17586725]
20. Gao S & Liu F Fetal liver: an ideal niche for hematopoietic stem cell expansion. Sci China Life Sci 61, 885–892 (2018). [PubMed: 29934917]
21. Hackney JA et al. A molecular profile of a hematopoietic stem cell niche. Proc Natl Acad Sci U S A 99, 13061–13066 (2002). [PubMed: 12226475]
22. Zhang CC et al. Angiopoietin-like proteins stimulate ex vivo expansion of hematopoietic stem cells. Nat Med 12, 240–245 (2006). [PubMed: 16429146]
23. Zhang CC, Kaba M, Iizuka S, Huynh H & Lodish HF Angiopoietin-like 5 and IGFBP2 stimulate ex vivo expansion of human cord blood hematopoietic stem cells as assayed by NOD/SCID transplantation. Blood 111, 3415–3423 (2008). [PubMed: 18202223]
24. Bowman TV & Zon LI Lessons from the Niche for Generation and Expansion of Hematopoietic Stem Cells. Drug Discov Today Ther Strateg 6, 135–140 (2009). [PubMed: 21212834]
25. Moore KA, Pytowski B, Witte L, Hicklin D & Lemischka IR Hematopoietic activity of a stromal cell transmembrane protein containing epidermal growth factor-like repeat motifs. Proc Natl Acad Sci U S A 94, 4011–4016 (1997). [PubMed: 9108096]
26. Chou S & Lodish HF Fetal liver hepatic progenitors are supportive stromal cells for hematopoietic stem cells. Proc Natl Acad Sci U S A 107, 7799–7804 (2010). [PubMed: 20385801]
27. Mahony CB & Bertrand JY How HSCs Colonize and Expand in the Fetal Niche of the Vertebrate Embryo: An Evolutionary Perspective. Front Cell Dev Biol 7, 34 (2019). [PubMed: 30915333]
28. Ganuza M, Hall T, Obeng EA & McKinney-Freeman S Clones assemble! The clonal complexity of blood during ontogeny and disease. Exp Hematol (2020).
29. Murayama E et al. Tracing hematopoietic precursor migration to successive hematopoietic organs during zebrafish development. Immunity 25, 963–975 (2006). [PubMed: 17157041]
30. Khan JA et al. Fetal liver hematopoietic stem cell niches associate with portal vessels. Science 351, 176–180 (2016). [PubMed: 26634440]
31. Deng M et al. A motif in LILRB2 critical for Angptl2 binding and activation. Blood 124, 924–935 (2014). [PubMed: 24899623]
32. Charbord P & Moore K Gene expression in stem cell-supporting stromal cell lines. Ann N Y Acad Sci 1044, 159–167 (2005). [PubMed: 15958709]
33. Fujio K, Evarts RP, Hu Z, Marsden ER & Thorgeirsson SS Expression of stem cell factor and its receptor, c-kit, during liver regeneration from putative stem cells in adult rat. Lab Invest 70, 511–516 (1994). [PubMed: 7513770]
34. Kubota H, Yao HL & Reid LM Identification and characterization of vitamin A-storing cells in fetal liver: implications for functional importance of hepatic stellate cells in liver development and hematopoiesis. Stem Cells 25, 2339–2349 (2007). [PubMed: 17585172]
35. Tan KS, Kulkeaw K, Nakanishi Y & Sugiyama D Expression of cytokine and extracellular matrix mRNAs in fetal hepatic stellate cells. Genes Cells 22, 836–844 (2017). [PubMed: 28776905]
36. Sugimura R et al. Haematopoietic stem and progenitor cells from human pluripotent stem cells. Nature 545, 432–438 (2017). [PubMed: 28514439]
37. Lis R et al. Conversion of adult endothelium to immunocompetent haematopoietic stem cells. Nature 545, 439–445 (2017). [PubMed: 28514438]
38. Wilkinson AC et al. Long-term ex vivo haematopoietic-stem-cell expansion allows nonconditioned transplantation. Nature 571, 117–121 (2019). [PubMed: 31142833]
39. Catlin SN, Busque L, Gale RE, Guttorp P & Abkowitz JL The replication rate of human hematopoietic stem cells in vivo. Blood 117, 4460–4466 (2011). [PubMed: 21343613]

40. Werner B et al. Reconstructing the in vivo dynamics of hematopoietic stem cells from telomere length distributions. Elife 4 (2015).
41. Lee-Six H et al. Population dynamics of normal human blood inferred from somatic mutations. Nature 561, 473–478 (2018). [PubMed: 30185910]
42. Ganuza M et al. The global clonal complexity of the murine blood system declines throughout life and after serial transplantation. Blood 133, 1927–1942 (2019). [PubMed: 30782612]
43. Snippert HJ et al. Intestinal crypt homeostasis results from neutral competition between symmetrically dividing Lgr5 stem cells. Cell 143, 134–144 (2010). [PubMed: 20887898]
44. Ruzankina Y et al. Deletion of the developmentally essential gene ATR in adult mice leads to age-related phenotypes and stem cell loss. Cell Stem Cell 1, 113–126 (2007). [PubMed: 18371340]
45. Tumbar T et al. Defining the epithelial stem cell niche in skin. Science 303, 359–363 (2004). [PubMed: 14671312]
46. Hochedlinger K, Yamada Y, Beard C & Jaenisch R Ectopic expression of Oct-4 blocks progenitor-cell differentiation and causes dysplasia in epithelial tissues. Cell 121, 465–477 (2005). [PubMed: 15882627]
47. Beaudin AE et al. A Transient Developmental Hematopoietic Stem Cell Gives Rise to Innate-like B and T Cells. Cell Stem Cell 19, 768–783 (2016). [PubMed: 27666010]
48. Sun J et al. Clonal dynamics of native haematopoiesis. Nature 514, 322–327 (2014). [PubMed: 25296256]
49. Rodriguez-Fraticelli AE et al. Clonal analysis of lineage fate in native haematopoiesis. Nature 553, 212–216 (2018). [PubMed: 29323290]
50. Busch K et al. Fundamental properties of unperturbed haematopoiesis from stem cells in vivo. Nature 518, 542–546 (2015). [PubMed: 25686605]
51. Kim I, He S, Yilmaz OH, Kiel MJ & Morrison SJ Enhanced purification of fetal liver hematopoietic stem cells using SLAM family receptors. Blood 108, 737–744 (2006). [PubMed: 16569764]
52. Harrison DE, Zhong RK, Jordan CT, Lemischka IR & Astle CM Relative to adult marrow, fetal liver repopulates nearly five times more effectively long-term than short-term. Exp Hematol 25, 293–297 (1997). [PubMed: 9131003]
53. Bernitz JM, Kim HS, MacArthur B, Sieburg H & Moore K Hematopoietic Stem Cells Count and Remember Self-Renewal Divisions. Cell 167, 1296–1309 e1210 (2016). [PubMed: 27839867]
54. Passegue E, Wagers AJ, Giuriato S, Anderson WC & Weissman IL Global analysis of proliferation and cell cycle gene expression in the regulation of hematopoietic stem and progenitor cell fates. J Exp Med 202, 1599–1611 (2005). [PubMed: 16330818]
55. Ikuta K & Weissman IL Evidence that hematopoietic stem cells express mouse c-kit but do not depend on steel factor for their generation. Proc Natl Acad Sci U S A 89, 1502–1506 (1992). [PubMed: 1371359]
56. Hinge A et al. p190-B RhoGAP and intracellular cytokine signals balance hematopoietic stem and progenitor cell self-renewal and differentiation. Nat Commun 8, 14382 (2017). [PubMed: 28176763]
57. Bowie MB et al. Identification of a new intrinsically timed developmental checkpoint that reprograms key hematopoietic stem cell properties. Proc Natl Acad Sci U S A 104, 5878–5882 (2007). [PubMed: 17379664]
58. Kiel MJ et al. SLAM family receptors distinguish hematopoietic stem and progenitor cells and reveal endothelial niches for stem cells. Cell 121, 1109–1121 (2005). [PubMed: 15989959]
59. Yilmaz OH, Kiel MJ & Morrison SJ SLAM family markers are conserved among hematopoietic stem cells from old and reconstituted mice and markedly increase their purity. Blood 107, 924–930 (2006). [PubMed: 16219798]
60. Takano H, Ema H, Sudo K & Nakauchi H Asymmetric division and lineage commitment at the level of hematopoietic stem cells: inference from differentiation in daughter cell and granddaughter cell pairs. J Exp Med 199, 295–302 (2004). [PubMed: 14744992]
61. Hamey FK & Gottgens B Machine learning predicts putative hematopoietic stem cells within large single-cell transcriptomics data sets. Exp Hematol 78, 11–20 (2019). [PubMed: 31513832]

62. Haltalli MLR et al. Manipulating niche composition limits damage to haematopoietic stem cells during Plasmodium infection. Nat Cell Biol 22, 1399–1410 (2020). [PubMed: 33230302]

63. Medvinsky AL & Dzierzak EA Development of the definitive hematopoietic hierarchy in the mouse. Dev Comp Immunol 22, 289–301 (1998). [PubMed: 9700459]

64. Boitano AE et al. Aryl hydrocarbon receptor antagonists promote the expansion of human hematopoietic stem cells. Science 329, 1345–1348 (2010). [PubMed: 20688981]

65. Wagner JE Jr. et al. Phase I/II Trial of StemRegenin-1 Expanded Umbilical Cord Blood Hematopoietic Stem Cells Supports Testing as a Stand-Alone Graft. Cell Stem Cell 18, 144–155 (2016). [PubMed: 26669897]

66. Fares I et al. Cord blood expansion. Pyrimidoindole derivatives are agonists of human hematopoietic stem cell self-renewal. Science 345, 1509–1512 (2014). [PubMed: 25237102]

67. Sadler TW Langman's Medical Embryology. . (2006).

68. Li Y et al. Single-Cell Analysis of Neonatal HSC Ontogeny Reveals Gradual and Uncoordinated Transcriptional Reprogramming that Begins before Birth. Cell Stem Cell 27, 732–747 e737 (2020). [PubMed: 32822583]

69. Pei W et al. Polylox barcoding reveals haematopoietic stem cell fates realized in vivo. Nature 548, 456–460 (2017). [PubMed: 28813413]

70. Oguro H, Ding L & Morrison SJ SLAM family markers resolve functionally distinct subpopulations of hematopoietic stem cells and multipotent progenitors. Cell Stem Cell 13, 102–116 (2013). [PubMed: 23827712]

Methods-only References

71. Todaro GJ & Green H Quantitative studies of the growth of mouse embryo cells in culture and their development into established lines. J Cell Biol 17, 299–313 (1963). [PubMed: 13985244]

72. Benjamini Y, and Hochberg Y Controlling the false discovery rate: a practical and powerful approach to multiple testing. Journal of the Royal Statistical Society Series B 57, 289–300 (1995).

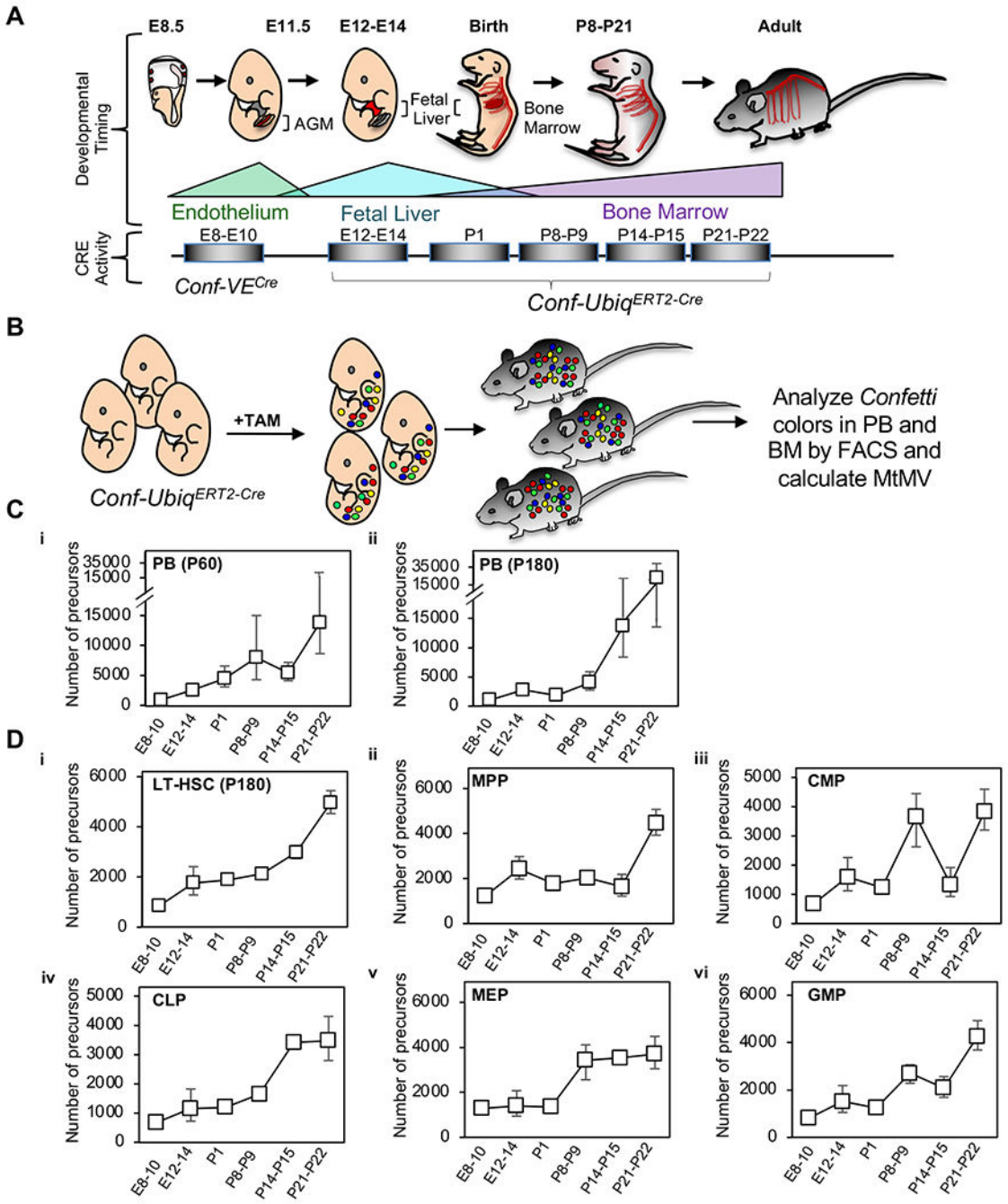

Figure 1. Life-long blood progenitor expansion in the fetal liver is modest.

A. Schematic to highlight developmental stages and windows of CRE activity (boxes). Triangles represent accumulation of transplantable HSC in each tissue. **B.** Experimental schematic. Blood and/or bone marrow was analyzed at P60 and P180 by flow cytometry to assess MtMV in each mouse cohort. **C.** Graphs show the MtMV-based estimates of numbers of progenitors contributing to PB at P60 (n≥8: E8-10, n=16; E12-14, n=18; P1, n=11; P8-9, n=18; P14-15, n=13; P21-22, n=8) (**Ci**) and P180 (n≥4: E8-10, n=5; E12-14, n=9; P1, n=11; P8-9, n=18; P14-15, n=13; P21-22, n=4) (**Cii**). **D.** Graphs show the

MtMV-based estimates of numbers of progenitors contributing to BM HSPCs [long-term (LT)-HSC, MPP, CMP, CLP, MEP, GMP] at P180 (n ≥6: E8-10, n=5; E12-14, n=12; P1, n=11; P8-9, n=7; P14-15, n=13; P21-22, n=14) labelled at distinct windows of ontogeny. Numbers were estimated by MtMV among cohorts of $ROSA26^{+/Confetti}VE^{+/T}$ (at E8-10) and TAM-treated $ROSA26^{+/Confetti}Ubiq^{+/T}$ mice at the indicated time points. Results reflect the analysis of mice of both sexes. Error bars indicate the 95% confidence intervals. See also Supplementary Table 1.

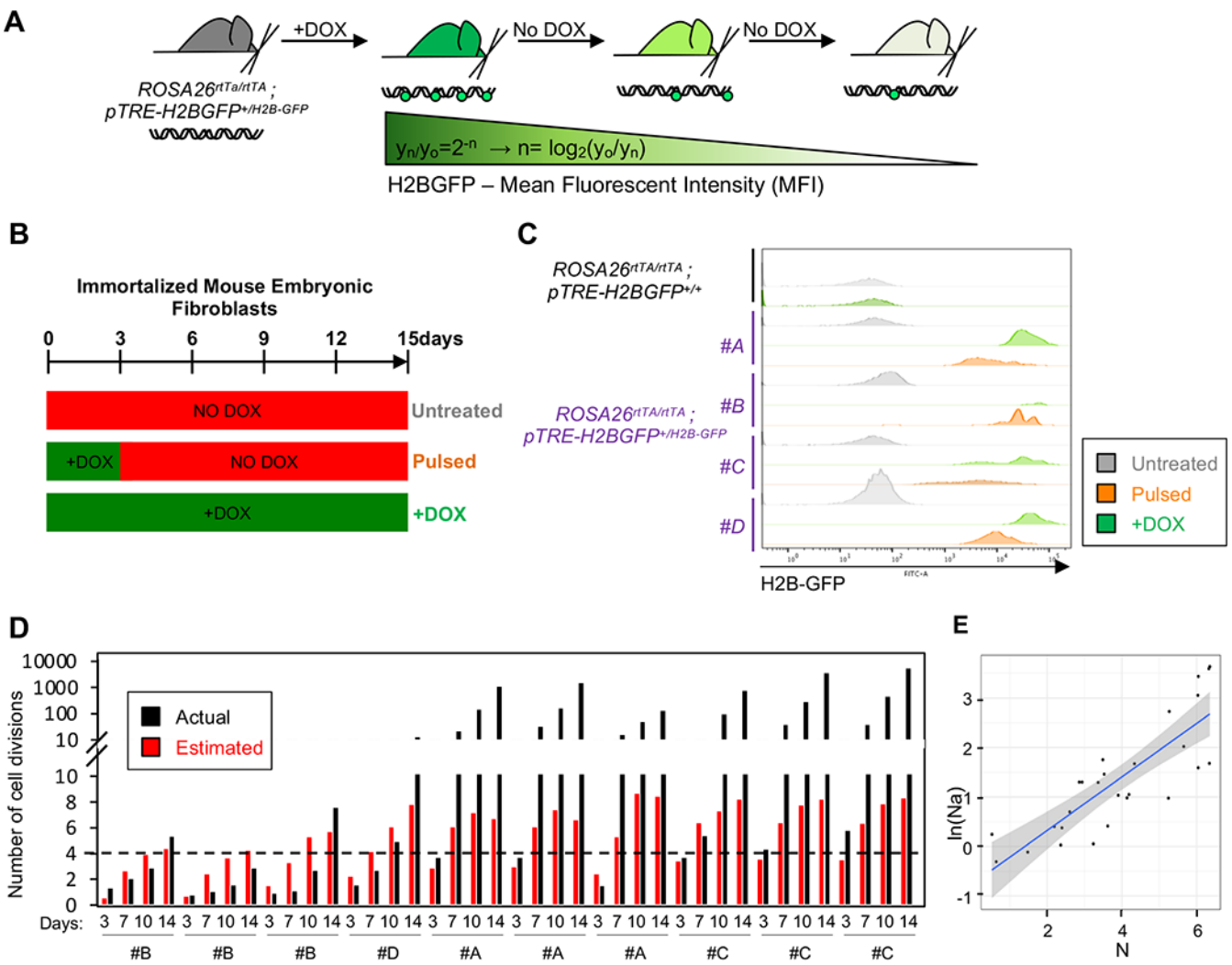

Figure 2. Validation of the utility of the *ROSA26*$^{rtTa/rtTA}$*pTRE-H2BGFP*$^{+/GFP}$ model for tracking cell divisions.

A. Schematic of kinetics of H2B-GFP signal dilution. DOX-treated *ROSA26*$^{rtTa/rtTA}$*; pTRE-H2BGFP*$^{+/GFP}$ mice express and accumulate H2B-GFP in their DNA. On DOX removal, H2B-GFP MFI is reduced by half with each cell division: $y_N/y_o=2^{-N}$ (y_o = initial H2B-GFP MFI; N = number of divisions, y_N = H2B-GFP MFI after N divisions). **B-E.** Analysis of the relationship between GFP MFI attrition and number of divisions after DOX removal using *ROSA26*$^{rtTa/rtTA}$*pTRE-H2BGFP*$^{+/GFP}$ MEFs. Immortalized *ROSA26*$^{rtTa/rtTA}$*pTRE-H2BGFP*$^{+/GFP}$ and *ROSA26*$^{rtTa/rtTA}$*pTRE-H2BGFP*$^{+/+}$control MEFs were cultured in the presence (+DOX) or absence of DOX (Untreated). After three days, DOX was removed (pulsed)**. B.** Experimental schematic. **C.** Representative flow cytometry analysis of four independent *ROSA26*$^{rtTa/rtTA}$*pTRE-H2BGFP*$^{+/GFP}$ cell lines. *ROSA26*$^{rtTa/rtTA}$*pTRE-H2BGFP*$^{+/+}$ control cells are also shown. Gray (untreated), green (+DOX), orange (pulsed, three days post-DOX removal). **D.** Four independent *ROSA26*$^{rtTa/rtTA}$*pTRE-H2BGFP*$^{+/GFP}$ cell lines were assayed in two independent experiments for 14 days. Upper Y-axis in logarithmic scale, bottom in linear scale. The actual number of cell divisions measured by

manual counting (black bars) and estimated via GFP MFI loss (red bars) are shown. **E.** Linear relationship between ln(Na) and N. ln(Na)= −0.757+0.541*N for N<6.5. Adjusted R-squared=0.6773. Gray area indicates standard error bands.

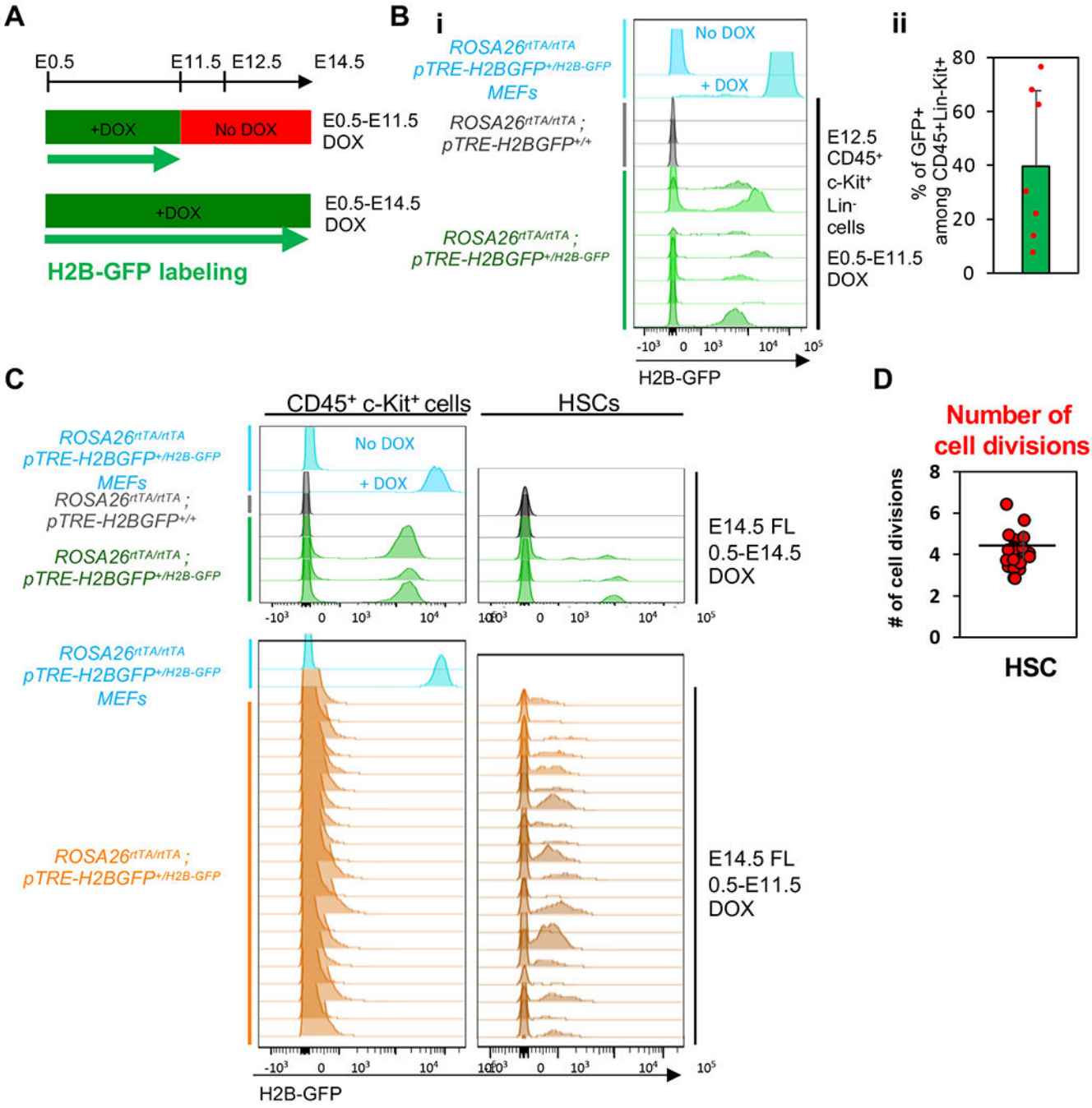

Figure 3. Phenotypic FL-HSCs undergo many cell divisions.

A. Experimental schematic. *ROSA26$^{rtTa/rtTA}$; pTRE-H2BGFP$^{+/GFP}$ and ROSA26$^{rtTa/rtTA}$; pTRE-H2BGFP$^{+/+}$* murine embryos were DOX-treated from E0.5-E11.5 or E0.5-E14.5. **Bi.** Representative flow cytometry histograms of GFP labelling in CD45^{+}c-Kit^{+}Lin^{-} cells at E12.5 in DOX-treated *ROSA26$^{rtTa/rtTA}$; pTRE-H2BGFP$^{+/+}$* (gray, n=3) and *ROSA26$^{rtTa/rtTA}$; pTRE-H2BGFP$^{+/GFP}$* (green, n=7) embryos. Untreated (No DOX) and DOX-treated (+DOX) *ROSA26$^{rtTa/rtTA}$; pTRE-H2BGFP$^{+/GFP}$* MEFs are light blue. **Bii.** % of GFP^{+} among CD45^{+}Lin^{-}Kit^{+} cells in E12.5 DOX-treated *ROSA26$^{rtTa/rtTA}$; pTRE-*

H2BGFP$^{+/GFP}$ embryos. **C.** *ROSA26*$^{rtTa/rtTA}$*; pTRE-H2BGFP*$^{+/GFP}$ embryos were exposed to DOX until E14.5 (green, n=3) or E11.5 (orange, n=20). GFP labelling of CD45^{+}c-Kit^{+}Lin^{-} cells (left panels) and HSCs (CD150^{+}CD48^{-}Lin^{-}Sca-1^{+}c-Kit^{+} cells; where Lin^{-}: TER119^{-}, Gr1^{-}, CD4^{-}, CD8^{-}, B220^{-}) (right panels) at E14.5. *ROSA26*$^{rtTa/rtTA}$*; pTRE-H2BGFP*$^{+/+}$negative control (gray), as well as untreated and DOX-treated *ROSA26*$^{rtTa/rtTA}$*; pTRE-H2BGFP*$^{+/GFP}$ control MEFs (n=4/each, light blue) are shown. **D.** Estimates of the number of actual cell divisions (N_a) encountered by E12.5 CD45^{+}c-Kit^{+}Lin^{-} (n=7) to yield E14.5 CD45^{+}c-Kit^{+}Lin^{-} and E14.5 HSCs (n=20) based on $N_a = e^{(-0.757+0.541*N)}$, where $N = \log_2(y_o/y_N)$ and calculated based on loss of GFP-MFI (Figure 2). Embryos represent six litters in two experiments. **Bii & D**. Each dot represents an independent embryo. Results reflect the analysis of mouse embryos at the indicated developmental stages. Sex of the embryos was not determined. Averages and standard deviations are shown.

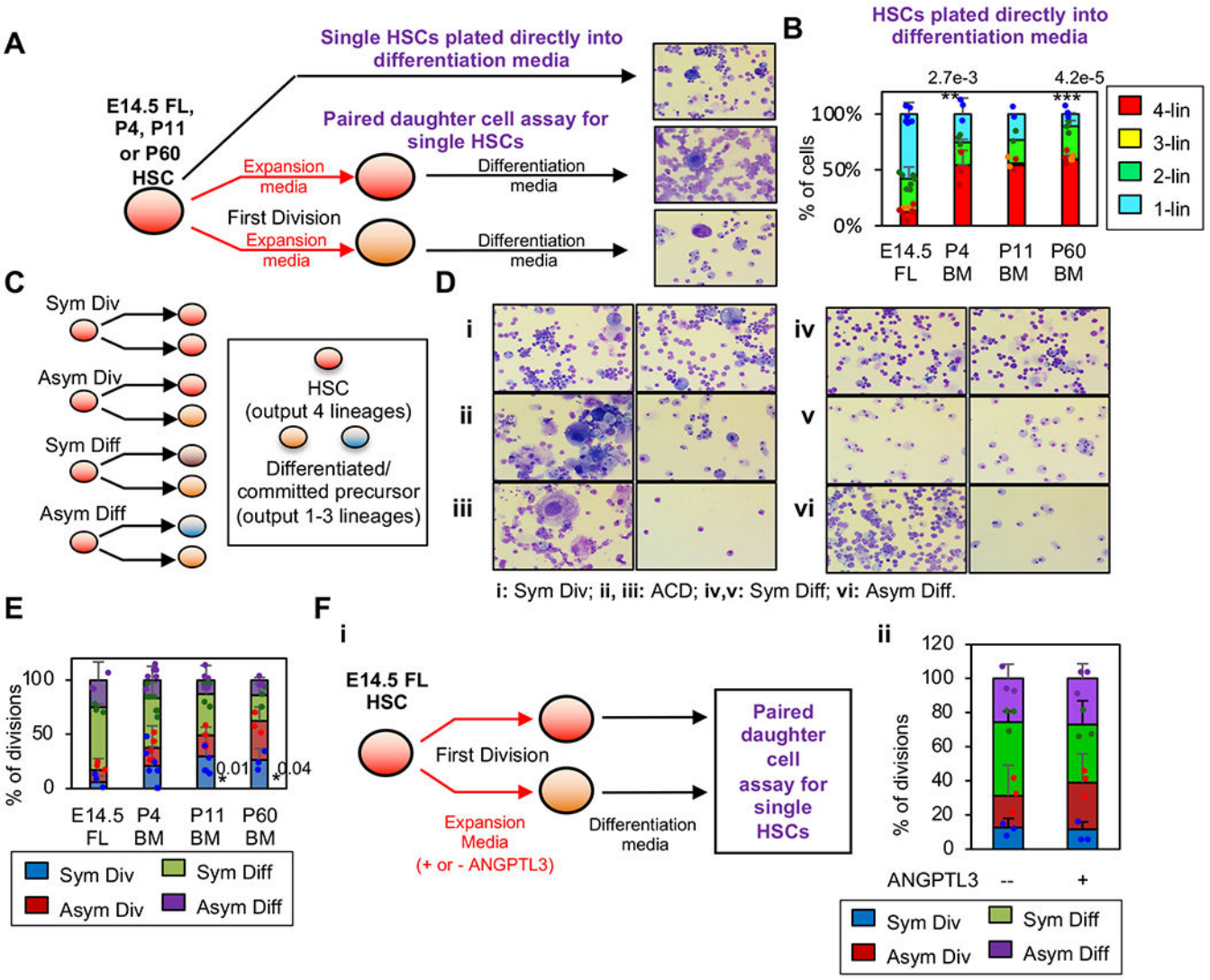

Figure 4. E14.5 FL HSC progenitors are biased to differentiate.

A. Experimental schematic. CD150^{+}CD48^{-}Lin^{-}Sca-1^{+}c-Kit^{+} C57Bl/6 HSCs were isolated from E14.5, P4, P11 or P60 mice of both sexes and plated in differentiation or expansion media. For expansion cultures, daughters of first cell division are separated and re-plated into differentiation media. **A-F.** Lin^{-}: TER119^{-}, Gr1^{-}, CD4^{-}, CD8^{-}, B220^{-}. **B.** Erythro-myeloid potential of E14.5 FL (n=143 cells from seven independent samples), P4 (n=113 cells, three independent samples), P11 (n=48 cells from two independent samples) and P60 HSC (n=113 cells from three independent samples). Data was collected in five independent experiments. % of HSCs generating 4, 3, 2 or 1 lineages is shown. **C-F.** Paired daughter cell assay. **C.** Schematic of potential outputs: asymmetric division, symmetric division, asymmetric differentiation or symmetric differentiation. **E.** Analysis of the output of first division undergone by E14 (n=41 cells, three independent samples), P4 (n=30 cells, seven independent samples), P11 (n=36 cells, six independent samples) and P60 HSCs (n=22 cells, three independent samples). **F.** Analysis of the output of first division undergone by E14.5-FL-HSCs cultured in the presence or absence of ANGPTL3 during a first division in

expansion media. **Fi.** Experimental schematic. **Fii.** Three independent biological replicates (n≥12 cell divisions analyzed/condition, two independent experiments). **B-F.** Means and individual values are depicted. Multivariate analysis of variance was used to compare percent of cells by different conditions. FDR was used to adjust for multiple testing corrections. Error bars show standard deviations. *** p-value <0.001. ** p-value <0.01. * p-value <0.05. Exact p-values are shown by graphs. **A&D.** Representative images of May-Grünwald-Giemsa stained cytospins from paired-daughters. Scale bar: 100μm. Cytospins were performed for each and every experiment and replicate detailed in B, E-Fii.

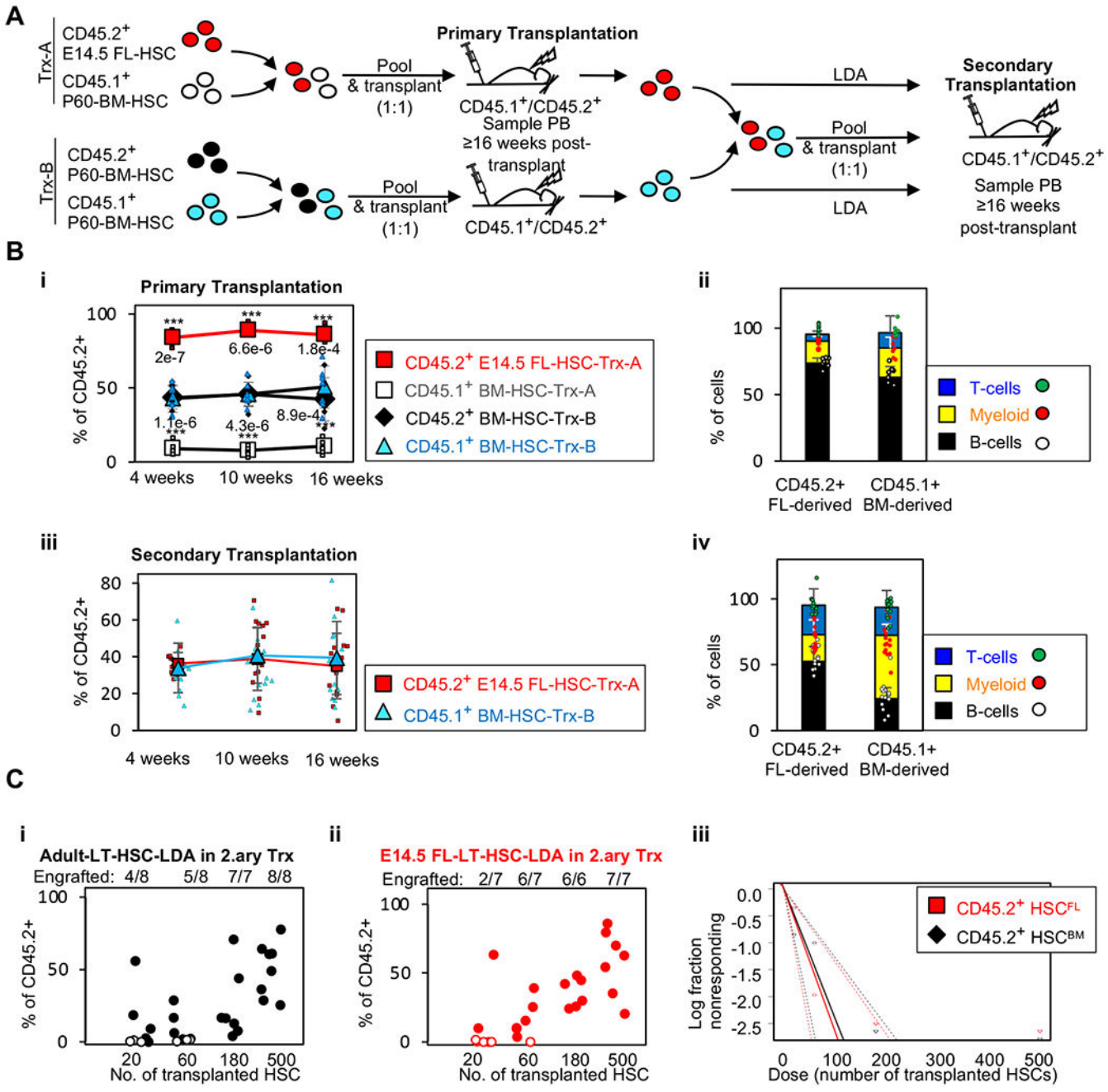

Figure 5. E14.5 FL HSC progenitors are biased to differentiate.

A. Transplantation strategy. **B.** Serial competitive transplantation of CD45.2$^+$E14.5 FL-HSC *versus* CD45.1$^+$adult-BM-HSC. %CD45.2$^+$ chimerism at 16 weeks post-transplant in (**Bi)** primary recipients (n=7/group) and **(Biii)** secondary (n=14/group) recipients. Distribution of T, B, and myeloid PB lineages in primary (**Bii)** and secondary (**Biv)** recipients of CD45.2$^+$ FL-HSCs and CD45.1$^+$ BM-HSCs 16 weeks post-transplantation. **C.** %CD45.2$^+$ chimerism in recipients of P60-BM-HSC (**Ci)** and of E14.5 FL-HSC (**Cii)** for LDA secondary transplants (n≥6/group). **B-Cii.** Individual data points and means are shown. Error bars denote standard deviations Each circle represents an individual recipient mouse. **Ci-ii.**

Non-engrafted mice are depicted as empty circles. Number of mice engrafted/number of recipients at each cell dose is depicted. **Ciii**. Log of the non-responding fraction is shown for each LDA cell dose from CD45.2^{+}E14.5 FL-HSC (CD45.2^{+} HSC^{FL}) and CD45.2^{+}adult-BM-HSC (CD45.2^{+} HSC^{BM}). Multivariate analysis of variance was used to compare percent of cells by different conditions. FDR was used to adjust for multiple testing corrections. ***p-value <0.001. Exact p-values are shown by graphs. Statistical differences related to CD45.2^{+} BM-HSC-Trx-B in **B.** 8-10 weeks old mice of both sexes were used as recipients.

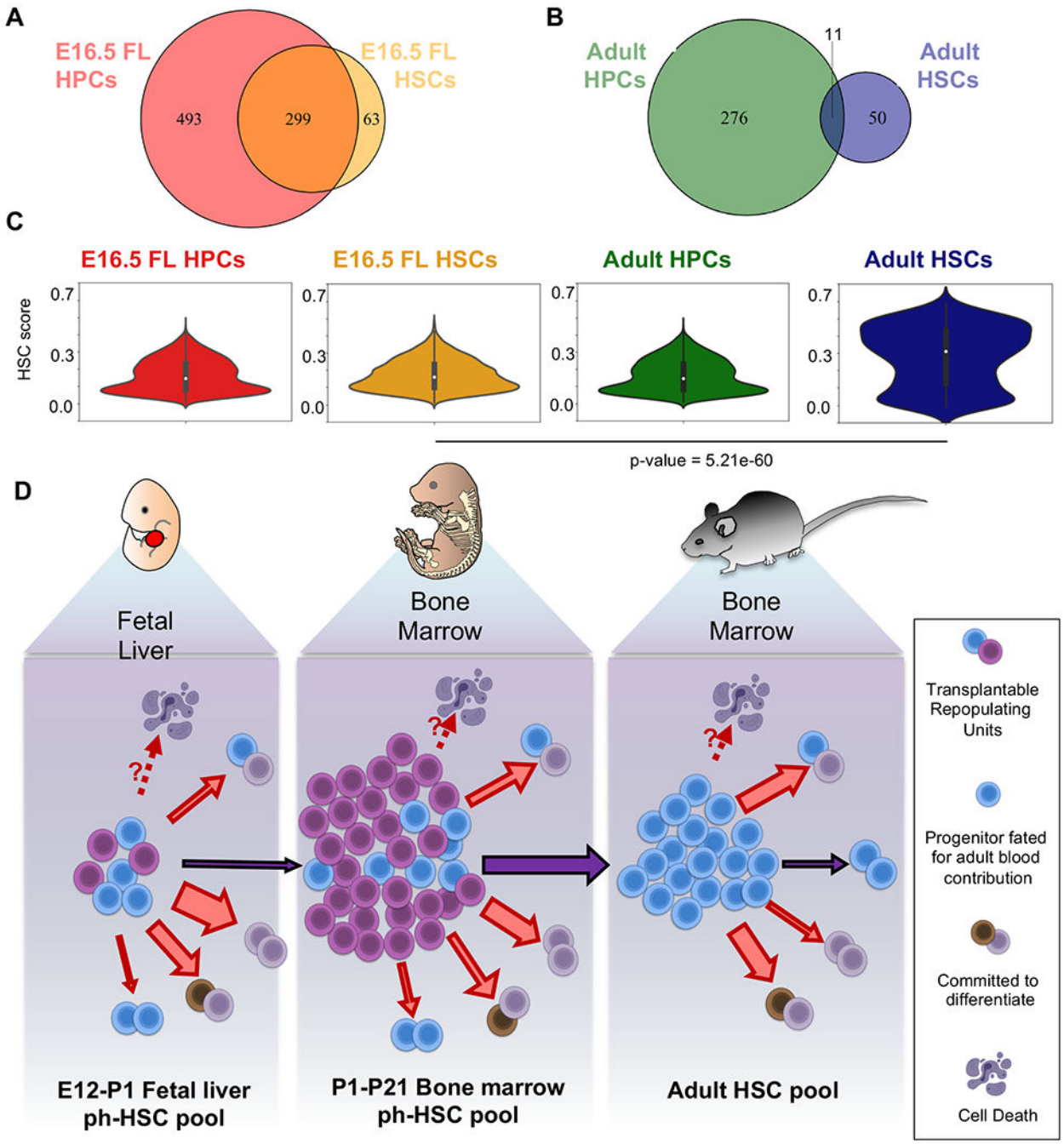

Figure 6. E16.5 FL-HSC are transcriptionally different from Adult HSCs. Updated model of the role of the FL niche in HSC ontogeny.

Single cell transcriptional profiling of E16.5 fetal and adult HPCs and HSCs (GSE128761) illustrate a unique signature of the adult HSC not observed in the E16.5 FL HSC. **A.** Venn diagram of E16.5FL HPC and E16.5 FL HSC marker genes that define the observed transcriptional heterogeneity with 83% of HSC marker genes present in the E16.5 FL HPC. **B.** Venn diagram of Adult HPC and Adult HSC marker genes that define the observed transcriptional heterogeneity with only 11 (18%) of HSC marker genes present

in the adult HPC. **A-B.** Marker genes provided in Source Data Figure 6. **C.** Distribution of hscScores for E16.5 HPC, E16.5 HSC, Adult HPC, and Adult HSC illustrate that the fetal HSCs are significantly (A two-sided Wilcoxon rank sum test p-value = 5.21e-60) different than adult HSCs. Strikingly, the fetal hscScore distribution resembles both fetal and adult HPC distributions. Boxplots depict the following values: minimum, first quartile, median, third quartile and maximum. **D.** Updated model of the role of the FL niche in HSC ontogeny. Large numbers of HSC progenitors are present in the murine embryos before the first transplantable HSC is detected at E10.5[7]. Although E12 phenotypic FL-HSC progenitors (ph-HSC) actively divide, they are biased to differentiate. Our data supports a model in which the rapid surge in repopulating units during FL ontogeny results from a combination of the maturation of immature pre-HSCs and some expansion of phenotypic LT-HSCs. As ontogeny progresses, the differentiation/self-renewal balance shifts towards less differentiation, which allows life-long HSCs to further accumulate with time before becoming quiescent[16].